

# Discovery of a Large $\sim 200$ kpc Gaseous Nebula at $z \approx 2.7$ with the *Spitzer Space Telescope*

Arjun Dey<sup>1</sup>, Chao Bian<sup>2</sup>, Baruch T. Soifer<sup>2,3</sup>, Kate Brand<sup>1</sup>, Michael J. I. Brown<sup>1,4</sup>, Frederic H. Chaffee<sup>5</sup>, Emeric LeFloc'h<sup>6</sup>, Grant Hill<sup>5</sup>, James R. Houck<sup>7</sup>, Buell T. Jannuzi<sup>1</sup>, Marcia Rieke<sup>6</sup>, Daniel Weedman<sup>7</sup>, Mark Brodwin<sup>8</sup>, Peter Eisenhardt<sup>8</sup>

## ABSTRACT

We report the discovery of a very large, spatially extended Ly $\alpha$ -emitting nebula at  $z = 2.656$  associated with a luminous mid-infrared source. The bright mid-infrared source ( $F_{24\mu\text{m}} = 0.86$  mJy) was first detected in observations made using the Spitzer Space Telescope. Existing broad-band imaging data from the NOAO Deep Wide-Field Survey revealed the mid-infrared source to be associated with a diffuse, spatially extended, optical counterpart in the  $B_W$  band. Spectroscopy and further imaging of this target reveals that the optical source is an almost purely line-emitting nebula with little, if any, detectable diffuse continuum emission. The Ly $\alpha$  nebula has a luminosity of  $L_{\text{Ly}\alpha} \approx 1.7 \times 10^{44}$  erg s<sup>-1</sup> and an extent of at least  $20''$  (160 kpc). Its central  $\approx 8''$  shows an ordered, monotonic velocity profile; interpreted as rotation, this region encloses a mass  $M \approx 6 \times 10^{12} M_{\odot}$ . Several sources lie within the nebula. The central region of the nebula shows narrow ( $\approx 365$  km s<sup>-1</sup>) emission lines of C IV and He II. The mid-infrared source is a compact object lying within the nebula, but offset from the

---

<sup>1</sup>National Optical Astronomy Observatory, 950 N. Cherry Ave., Tucson, AZ 85719; dey@noao.edu

<sup>2</sup>California Institute of Technology, Pasadena, CA 91125

<sup>3</sup>Spitzer Science Center, California Institute of Technology, MS 220-6, Pasadena, CA 91125

<sup>4</sup>Dept. of Astrophysical Sciences, Peyton Hall, Princeton University, Princeton, NJ 08544-1001

<sup>5</sup>W. M. Keck Observatory, 65-1120 Mamalahoa Hwy., Kamuela, HI 96743

<sup>6</sup>Steward Observatory, University of Arizona, Tucson, AZ 85721

<sup>7</sup>Astronomy Department, Cornell University, Ithaca, NY 14853

<sup>8</sup>Jet Propulsion Laboratory, California Institute of Technology, MC 169-327, 4800 Oak Grove Drive, Pasadena, CA 91109

center by a projected distance of  $\approx 2''.5$  (20 kpc), and likely to be an enshrouded AGN. A young star-forming galaxy lies near the northern end of the nebula. We suggest that the nebula is a site of recent multiple galaxy and AGN formation, with the spatial distribution of galaxies within the nebula perhaps tracking the formation history of the system.

*Subject headings:* galaxies:formation–galaxies:high-redshift–galaxies:starburst

## 1. Introduction

How do the most massive galaxies form? This is a question whose answer may provide one of the central tests of hierarchical galaxy formation theories. Our current theoretical paradigm suggests that the most massive galaxies form, like the rest of the galaxy population, by the hierarchical merging of smaller units and that this process occurs through the history of the universe. In seeming contrast, however, three lines of evidence suggest that at least some of the most massive galaxies may have had more dramatic origins. First, observations of the most massive galaxies at redshifts out to  $z \lesssim 1.5$  suggest that the bulk of the stars in these objects formed at much higher redshifts in a brief time period characterized by very high star-formation rates ( $\gtrsim 300 M_{\odot} \text{ yr}^{-1}$ ) (e.g., McCarthy et al. 2004). Second, the host galaxies of powerful radio sources, which appear to be dynamically relaxed massive ellipticals at redshifts out to one (e.g., Zirm et al. 2003), at higher redshifts ( $z \gtrsim 3$ ) are surrounded by large (100–200 kpc), luminous ( $> 10^{43} \text{ erg s}^{-1}$ ) Ly $\alpha$  nebulae and small, embedded, star-forming objects (e.g., Reuland et al. 2003). This suggests that these host galaxies are formed in a rather spectacular gravitational collapse event rather than by the slow build-up of many merging events over time (Reuland et al. 2003). The discovery of large, diffuse Ly $\alpha$  haloes in several surveys and their association with large galaxy overdensities adds further support to the idea that these haloes mark the formation sites of massive galaxies (e.g., Keel et al. 1999; Steidel et al. 2000; Francis et al. 2001; Palunas et al. 2004; Matsuda et al. 2004). Third, the recent discoveries that dust-enshrouded galaxies selected in sub-mm surveys have very large star-formation rates, large correlation length and high median redshift suggest that this population may represent the formation epoch of massive galaxies (e.g., Blain et al. 2004; Chapman et al. 2004). Taken together, the empirical picture that emerges for massive galaxy formation is one of a violent, perhaps brief epoch of dust-enshrouded star-formation followed by a more gradual unveiling of the galaxy by the dissipation of its dusty, gaseous envelope.

It is clearly of great interest, therefore, to find and characterize the formation sites of massive galaxies. Thus far we have been limited to studying the ( $>100$  kpc) Ly $\alpha$  halos

and environments of luminous radio galaxies, which may be affected in peculiar ways by the presence of the active galactic nucleus and its ejecta, and to the similarly large Ly $\alpha$  nebulae in two regions: four associated with a massive structure at  $z = 2.38$  (Francis et al. 2001; Palunas et al. 2004) and two others associated with a structure at  $z = 3.09$  (Steidel et al. 2000; Matsuda et al. 2004). It is worth noting that the only narrow-band emission line surveys that have yielded discoveries of these spectacular Ly $\alpha$  haloes have been targeted at large mass overdensities, so their mutual association may be misleading. Ground-based sub-mm surveys provide a less biased approach in principle, but so far have been limited by technology: the current suite of bolometer arrays provide poor positional accuracy and limited fields of view which are not suited to wide-field surveys.

In this paper, we present observations that suggest that mid-IR surveys with *Spitzer Space Telescope* may provide an alternate approach: we report on observations of a luminous, very spatially extended Ly $\alpha$  nebula at  $z = 2.6562$  discovered by virtue of its associated 24 $\mu$ m emission. We present the description of our observations of this nebula in §2 and our results and measurements in §3. In §4, we discuss the implications of this discovery on future studies of massive galaxy formation.

Throughout this paper we use  $H_0 = 70 \text{ km s}^{-1} \text{ Mpc}^{-1}$ ,  $\Omega_m = 0.3$ ,  $\Omega_\lambda = 0.7$ . At a redshift  $z = 2.6562$  the luminosity distance is  $d_L = 21.946 \text{ Gpc}$  and 1'' corresponds to a physical size of 7.96 kpc.

## 2. Observations

The optical photometry of this source is derived primarily from the images obtained by the NOAO Deep Wide-Field Survey (NDWFS<sup>1</sup>; Jannuzi & Dey 1999; Jannuzi et al. 2005; Dey et al. 2005). The NDWFS is a deep, ground-based, optical and near-infrared imaging survey of two 9.3 square degree fields, one in Boötes and one in Cetus, conducted using the 4m and 2.1m telescopes of the National Optical Astronomy Observatory. The survey is designed to study the evolution and clustering of galaxies over a wide range in redshift, and reaches median  $5\sigma$  point-source depths in the  $B_W$ ,  $R$ ,  $I$  and  $K$  bands of  $\approx 27.1$ , 26.1, 25.4 and 19.0 mag (Vega) respectively. The data products for the NDWFS will be described elsewhere (Dey et al. 2005; Jannuzi et al. 2005, in preparation). The specific optical image stacks used in this paper have  $B_W$ ,  $R$ , and  $I$  band exposure times of 2.67, 2.67 and 3.33 hours and reach  $5\sigma$  point-source depths of 27.31, 26.23 and 25.47 mag respectively. Stars in all three image stacks have  $\text{FWHM} \approx 1''$ . The source is undetected in the near-infrared  $K_S$

---

<sup>1</sup>See also <http://www.noao.edu/noaodeep/>

data of the NDWFS. The NDWFS astrometry is tied to the reference frame defined by stars from the USNO A-2 catalog (Monet et al. 1998).

The NDWFS Boötes field was mapped at 24, 70 and 160 $\mu$ m using the Multiband Imaging Photometer for Spitzer (MIPS; Rieke et al. 2004) in late January 2004 to  $1\sigma$  rms depths of 51 $\mu$ Jy, 5mJy and 18mJy respectively. The data were reduced by the MIPS GTO team. Details of the survey, including the mapping strategy, data reduction and the resulting catalog, will be discussed elsewhere (LeFloc’h et al. 2005, in preparation). The entire Boötes field was also mapped at 3.6, 4.5, 5.6 and 8.0 $\mu$ m using the Infrared Array Camera (IRAC; Fazio et al. 2004) on *Spitzer*; details of the IRAC observations may be found in Eisenhardt et al. (2004). Both the MIPS and IRAC data are astrometrically calibrated to the 2MASS astrometric frame.

Initial optical identifications of the MIPS sources with 24 $\mu$ m flux densities brighter than 0.75mJy were done using the image catalogs from the NDWFS. The MIPS 24 $\mu$ m sources are all unresolved at the 6'' angular resolution of the *Spitzer Space Telescope*. The images of all MIPS sources with optical associations fainter than  $I=23$  mag were visually inspected. A 24 $\mu$ m source SST24 J1434110+331733 with a flux density of 0.86mJy was found to lie within a faint, diffuse, spatially extended optical source with blue optical colors, which suggested that the colors may be the result of strong line emission in the  $B_W$  band.

Spectroscopic observations of the MIPS 24 $\mu$ m candidate SST24 J1434110+331733 were obtained using the Low Resolution Imaging Spectrometer (LRIS; Oke et al. 1995) on the Keck I telescope on U.T. 2004 May 21 and 2004 June 22. The first set of observations, four 30 min exposures, were obtained in 0.8'' seeing through a 1.0'' wide and 11'' long slitlet oriented at PA=0°. LRIS was configured with the 5600Å dichroic, the 400l/mm ( $\lambda_c=3400\text{Å}$ , 1.09Å pix<sup>-1</sup>) grism on the blue side and the 400l/mm ( $\lambda_b=8500\text{Å}$ , 1.86Å pix<sup>-1</sup>) grating on the red side. A second set of five 30 min observations were obtained in 1'' seeing through a 1.5'' wide and 30'' long slitlet oriented at PA=19.4°, with the 6800Å dichroic, 300l/mm ( $\lambda_c=5000\text{Å}$ , 1.43Å pix<sup>-1</sup>) grism, and the same red grating. In each observation set, the telescope was offset by a few arcsec between individual 30 min exposures. Relative spectrophotometric calibrations were performed using observations of Wolf 1346 (Oke 1990; Massey et al. 1988; Massey & Gronwall 1990). Figure 1 shows the location and orientation of the LRIS slitlets on the  $B_W$  image of the source.

Additional optical observations of the field were obtained using the MiniMOSAIC camera (“MiniMo”) on the WIYN 3.5-m telescope of the Kitt Peak National Observatory on the nights of U.T. 2004 June 14 – 17. A total of six 1200 s images were obtained through the 62Å-wide narrow-band filter centered at 4448Å (hereinafter NB4448, also called “W20” in the WIYN filter set; centered on the redshifted Ly $\alpha$  line) and three 900 s images were obtained

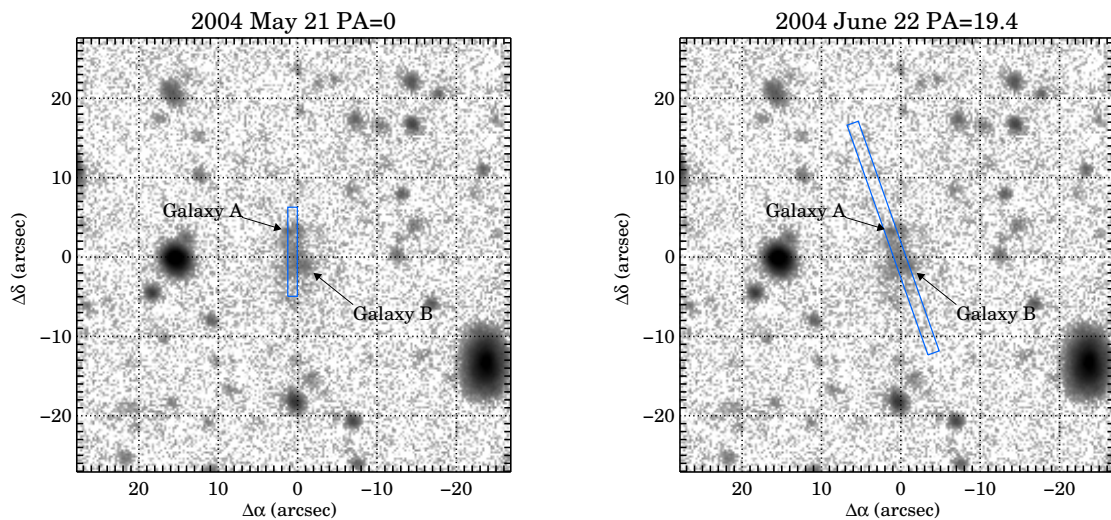


Fig. 1.— The left and right panels show the location, orientation and size of the LRIS slitlets superimposed on the  $B_W$  image of SST24 J1434110+331733. The origin corresponds to  $14^h34^m10^s.977 + 33^\circ17'30''.87$ , the centroid of the  $\text{Ly}\alpha$  emission as determined from the narrow-band image (please see text). Note that only the slitlet at PA=19.4 (on the right) includes light from galaxy B.

through a Gunn  $G$  filter. The seeing varied from night to night, but point sources in the final NB4448 and G-band image stacks have an effective FWHM of  $0''.7$  and  $0''.8$  respectively. The data were calibrated using observations of the spectrophotometric standard Feige 110 (Oke 1990; Stone 1977) through the NB4448 filter and Landolt field SA112 (Landolt 1992) through the Gunn  $G$  filter on photometric nights.

All the WIYN optical imaging data were astrometrically calibrated using the USNO A-2 catalog and tied to the same astrometric frame as the NDWFS imaging data. There is a small astrometric offset between the IRAC and MIPS 2MASS frame and the NDWFS/USNO A-2 frame of roughly  $0''.5$  which we corrected before comparing the Spitzer and ground-based data. All positions quoted here are on the NDWFS/USNO A-2 reference frame.

### 3. Results

#### 3.1. Morphology and Astrometry

Image cutouts of the  $B_W$ ,  $G$ ,  $R$  and  $I$  images are shown in figure 2, with the contour map from the NB4448 image overlaid on the  $I$ -band image<sup>2</sup>. The system is diffuse and relatively bright in the  $B_W$  band, which is largely dominated by the Ly $\alpha$  line emission; there is a fairly compact galaxy at its northern extent which is labelled ‘A’ in figure 2. In contrast to the  $B_W$  image, the  $G$ ,  $R$  and  $I$  band cutouts show only little (if any) diffuse emission, but do show some light associated with the regions ‘A’ and ‘B’. The Ly $\alpha$  emission appears to avoid ‘A’. The center of the Ly $\alpha$  emission lies near ‘B’, but slightly to its east; the spectrum of this central region is therefore contaminated by continuum emission from ‘B’.

The NDWFS astrometry is tied to a frame defined by moderately bright (12–17 mag) stars in the USNO A-2 catalog, whereas the MIPS astrometry is calibrated using 2MASS. Roughly 98% of the bright ( $F_{24\mu\text{m}} > 0.75$  mJy) MIPS sources have well determined optical counterparts in the NDWFS data, and comparisons of the relative astrometry between these MIPS and NDWFS matches show a small, but significant relative offset of  $\Delta\alpha = 0''.38$  and  $\Delta\delta = 0''.14$  between the two frames. The offset arises because of a small magnitude-dependent astrometric error internal to the USNO A-2 catalog (Monet et al. 2003). The MIPS source is located at  $14^{\text{h}}34^{\text{m}}10^{\text{s}}.958 + 33^{\circ}17'32''.57$  in the J2000 2MASS reference frame. In the optical reference frame of the NDWFS, the source position is  $14^{\text{h}}34^{\text{m}}10^{\text{s}}.988 + 33^{\circ}17'32''.71$  (J2000). Taking this offset into account, the MIPS source is found to lie on the northern end of the

---

<sup>2</sup>Larger finding charts of the field and astrometry of offset stars may be determined from image cutouts of the NDWFS available from the NOAO Science Archive (<http://www.archive.noao.edu/ndwfs/>).

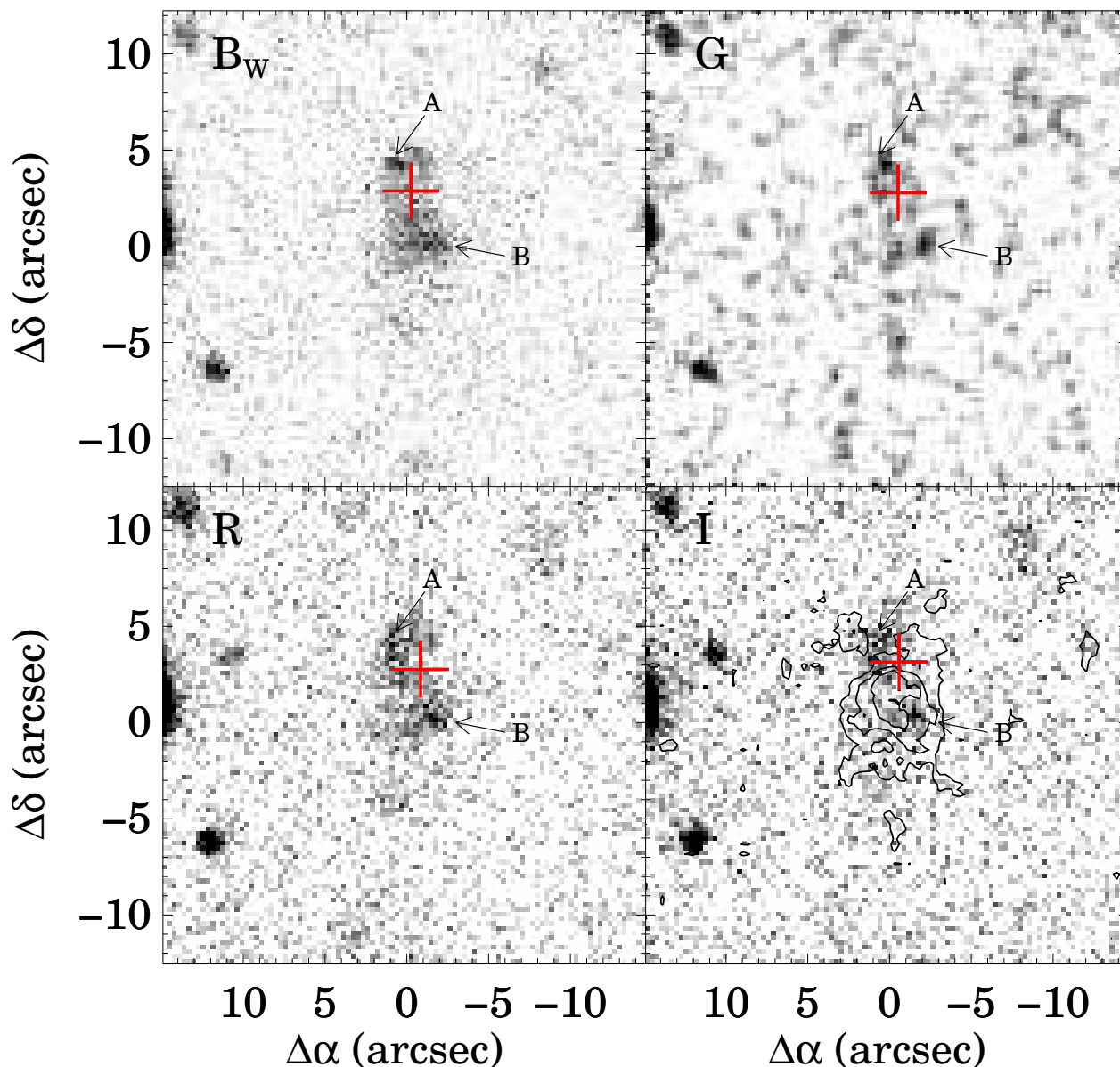


Fig. 2.— Image cutouts of the SST24 J1434110+331733 in  $B_W$ -,  $G$ -,  $R$ - and  $I$ -bands. The origin (0,0) in all panels is at  $14^h34^m11^s005 + 33^\circ17'29''.84$  (J2000). The red crosses in the four panels mark the location of the  $24\mu\text{m}$  source ( $B_W$  panel), the  $3.6\mu\text{m}$  source ( $G$  panel), the IRAC  $4.5\mu\text{m}$  source ( $R$  panel) and the  $8.0\mu\text{m}$  source ( $I$  panel). The position of the source in the MIPS  $24\mu\text{m}$  and IRAC bands agrees to  $< 0''.5$ . The contours in the  $I$  panel denote the emission detected in the NB4448 filter centered on the  $\text{Ly}\alpha$  emission line. The continuum emission in this filter has not been subtracted, but contributes less than 10% of the total flux at all radii. The contours drawn correspond to line flux surface brightnesses of approximately  $[0.2, 0.4, 0.6, 0.8] \times 10^{-16} \text{erg s}^{-1} \text{cm}^{-2} \text{arcsec}^{-2}$ .

diffuse emission observed in the NDWFS  $B_W$  and NB4448 images, just to the southwest of galaxy A (fig 2). The location of the MIPS source is marked by a cross, and is believed to be accurate to  $\approx 0''.5$ . It lies  $\approx 0''.8$  west and  $1''.6$  south of galaxy A and  $\approx 1''.1$  east and  $2''.6$  north of galaxy B. The Ly $\alpha$  emission is centered roughly  $2''.5$ , or 20 kpc (projected), away from the MIPS source.

The position of the IRAC source detected in the  $3.6\mu\text{m}$ ,  $4.5\mu\text{m}$ , and  $8\mu\text{m}$  bands agree with the MIPS  $24\mu\text{m}$  source position to  $<0''.5$ , and confirm the relative (non-central) location of the mid-infrared source within the Ly $\alpha$  nebula.

### 3.2. Photometry

Table 1 presents our photometric data on SST24 J1434110+331733. The optical photometry was measured in a large aperture of radius  $10''$  centered on the centroid of the Ly $\alpha$  halo. The flux in the  $B_W$  band is dominated by the Ly $\alpha$  emission, and the optical measurement aperture for all bands includes galaxies A and B. These optical measurements should therefore be strictly treated as upper limits to the continuum emission from the region. Higher spatial resolution imaging and spectroscopy along  $\text{PA}\approx 90^\circ$  will be necessary to disentangle the contribution of galaxy B and determine the true continuum contribution from sources within the nebula.

### 3.3. Redshifts of the Nebula and Coincident Sources

The spectroscopic observations reveal a very complex system within the extent of the nebula, comprised of several continuum sources. Figure 3 shows the two-dimensional spectrum recorded on the blue side of LRIS in  $\text{PA}=19.4^\circ$ , and figure 4 shows the extracted one-dimensional spectrum of the system obtained through a (wide)  $10''.9\times 1''.5$  aperture from these data. Emission line measurements are presented in table 2. The redshift of the system is well established at  $z = 2.6562$  through the detection of Ly $\alpha$ , C IV, He II and weak C III].

There are three main continuum contributors to this large-aperture spectrum: (i) galaxy A (figure 5), (ii) a source  $1''.6$  southwest of galaxy A along the  $\text{PA}=19.4^\circ$  slitlet which may be associated with the MIPS source (figure 6), and (iii) a source  $4''.7$  southwest of A, and close to the location of galaxy B (figure 7). We discuss each of these in turn.

The spectrum of galaxy A (figure 5) reveals a “Lyman-break galaxy” at a redshift of  $z \approx 2.656$ , characterized by a flat  $F_\nu$  continuum, interstellar absorption lines and no detectable Ly $\alpha$  emission. The interstellar absorption lines observed in typical Lyman-break

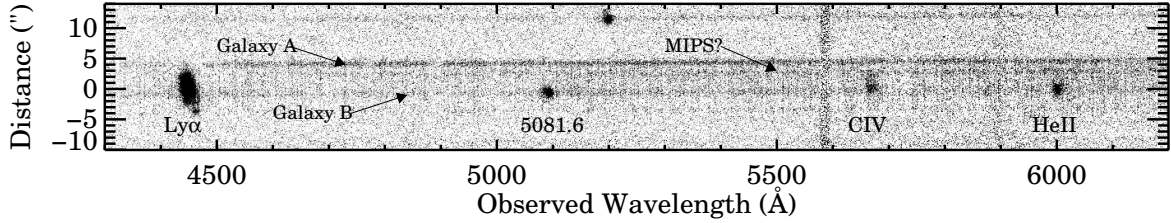


Fig. 3.— Two-dimensional spectrum of the Ly $\alpha$  nebula associated with SST24 J1434110+331733 obtained through a 1".5 wide slitlet oriented in PA=19.4 $^\circ$  and using LRIS-B on the Keck I telescope. The three continuum streaks and main emission lines are labelled. Please see text for details.

Table 1. Photometry of SST24 J1434110+331733

Band	Wavelength ( $\mu\text{m}$ )	Width ( $\mu\text{m}$ )	Aperture Center (J2000)	Aperture Radius	Magnitude (Vega)	$F_\nu$ ( $\text{erg s}^{-1} \text{cm}^{-2} \text{Hz}^{-1}$ )
NDWFS $B_W$	0.422	0.112	$14^h 34^m 10^s 977 + 33^\circ 17' 30'' 87$	10''	$22.64 \pm 0.05$	$3.18 \pm 0.15 \times 10^{-29}$
Gunn $G$	0.492	0.067	"	10''	$23.02 \pm 0.20$	$2.39 \pm 0.45 \times 10^{-29}$
NDWFS $R$	0.659	0.183	"	10''	$22.24 \pm 0.08$	$3.92 \pm 0.30 \times 10^{-29}$
NDWFS $I$	0.808	0.172	"	10''	$22.02 \pm 0.15$	$3.80 \pm 0.53 \times 10^{-29}$
NDWFS $K_S$	2.167	0.295	"	6''	$> 18.12^a$	$< 3.67 \times 10^{-28a}$
IRAC 3.6 $\mu\text{m}$	3.56	0.75	$14^h 34^m 10^s 979 + 33^\circ 17' 32'' 48$	6''	$17.83 \pm 0.13$	$2.04 \pm 0.24 \times 10^{-28}$
IRAC 4.5 $\mu\text{m}$	4.52	1.01	"	6''	$17.09 \pm 0.13$	$2.63 \pm 0.31 \times 10^{-28}$
IRAC 5.8 $\mu\text{m}$	5.73	1.42	"	6''	$15.93 \pm 0.36$	$4.97 \pm 1.66 \times 10^{-28}$
IRAC 8 $\mu\text{m}$	7.91	2.93	"	6''	$14.79 \pm 0.21$	$7.69 \pm 1.49 \times 10^{-28}$
MIPS 24 $\mu\text{m}$	24.0	5.3	$14^h 34^m 10^s 988 + 33^\circ 17' 32'' 71$	<sup>b</sup>	$9.83 \pm 0.06$	$8.56 \pm 0.51 \times 10^{-27}$
MIPS 70 $\mu\text{m}$	70.0	19.0				$< 2.5 \times 10^{-25}$
MIPS 160 $\mu\text{m}$	160.0	34.5				$< 9.0 \times 10^{-25}$
WSRT 1400MHz <sup>c</sup>	20cm		$14^h 34^m 10^s 78 + 33^\circ 17' 27'' 4$			$1.4 \pm 0.4 \times 10^{-27}$

<sup>a</sup>The  $K_S$  upper limit is  $2\sigma$  in a 6'' radius aperture.

<sup>b</sup>The MIPS photometry was determined using PSF-fitting techniques.

<sup>c</sup>WSRT measurement is from the deep 1400MHz survey of de Vries et al. (2002). The source is unresolved in the 13'' $\times$ 27'' beam.

galaxies can be blue shifted due to winds, and the redshift estimate based on these is therefore only good to  $\sim 1000 \text{ km s}^{-1}$ . The absorption line spectrum seen in figure 4 is almost entirely due to the continuum contribution from galaxy A to the large aperture extraction.

The spectrum of the second continuum source (figure 6) is quite red and shows weak C IV and C III] emission at  $z = 2.656$ , i.e., the redshift of the nebula. Its proximity to the MIPS  $24\mu\text{m}$  location suggests that it may be a star-forming galaxy reddened by dust. There are some possible continuum features visible in the spectrum of this source, that are consistent with a young, reddened star-forming object. No obvious emission lines uniquely due to an AGN are detected in this source.

The spectra of galaxy A and the MIPS source both show a fairly broad absorption feature at  $\lambda 5720\text{\AA}$ . The signal-to-noise ratio in this region is low, and sky subtraction using traditional fitting techniques on very extended faint objects can sometimes result in such features. If this feature is real, it is most likely to be due to a foreground absorption system, perhaps arising from either MgII $\lambda\lambda 2800$  at  $z \approx 1.04$  or an FeII  $2600\text{\AA}$  absorption complex at  $z \sim 1.20$ .”

The third continuum source (figure 7) is the most intriguing: it lies near the center of the Ly $\alpha$  nebula and apparently shows strong associated C IV and He II emission at the redshift of the nebula. This continuum source also shows an emission feature at  $5081.6\text{\AA}$ , the identification of which is uncertain. This feature is unlikely to be an emission line at the redshift of the Ly $\alpha$  nebula, since it does not match any strong features normally observed in high-redshift galaxies or AGN: at a rest wavelength of  $1389.9\text{\AA}$ , it could only be associated with blue-shifted SiIV $\lambda\lambda 1393.8, 1402.8$  emission, and would be the only feature with such a blue shift relative to the He II redshift, which seems very improbable. This spectral line also does not appear in the PA= $0^\circ$  spectrum, strongly suggesting that it is associated with galaxy B. Since the  $5081.6\text{\AA}$  line does not correspond to any normal species at the redshift of the Ly $\alpha$  nebula, we therefore suspect that galaxy B is an interloping system that does not lie at the redshift of the nebula. Given the asymmetry of the  $5081.6\text{\AA}$  emission line and the break in the continuum across the line, we suggest that galaxy B is a background source at a redshift of  $3.180$ . Galaxy B is located too far away from the centroid of the MIPS  $24\mu\text{m}$  emission and is therefore also not the source of the infrared emission. The spatial coincidence of the  $5081.6\text{\AA}$  feature and the He II and C IV emission lines in our spectrum must therefore be due to the unfortunate circumstance of the two contributing sources, the emission line source at  $z = 2.656$  and the background galaxy at  $z = 3.18$ , being located approximately along the short-axis of our slit, parallel to the dispersion direction. It is also likely that the continuum emission that we observe at this location is primarily due to galaxy B, and unrelated to the nebula.

The source near the top of the slit in figure 3 shows an asymmetric emission line at  $5188.5\text{\AA}$  and a break across the line; this emission line is consistent with  $\text{Ly}\alpha$  at a redshift of 3.268, and this galaxy is also a background source.

We are left, therefore, with the interpretation that two unrelated background sources are present in this  $1''.5 \times 30''$  slitlet, both at redshifts above three. We are confident the emission line detections associated with these objects are not instrumental effects, since they repeat on all the individual exposures and move in concert with their associated continuum when the targets were offset along the slit. It is not exceptional to find a serendipitous source with  $z > 3$  during LRIS spectroscopy; our experience is that one such source appears in about 15% of the masks used. Given the surface density of  $z \sim 3$  Lyman break galaxies ( $\approx 1.2$  per sq. arcmin for  $R \leq 25.5$  mag; (Steidel et al. 2003)), the Poisson probability of finding 2 in a single mask is 1.8%, and in a single slitlet is 0.01%. Note that these are lower limits to the probabilities since  $z \sim 3$  Lyman break galaxies are clustered. The redshift separation between the two background galaxies suggests a minimum comoving relative distance of  $\approx 80$  Mpc. Further spectroscopy of this region is clearly of interest in order to understand the field galaxy redshift distribution.

### 3.4. Spatial Extent of the $\text{Ly}\alpha$ Nebula

A visual examination of the NB4448 image at a hard stretch shows that the high surface brightness portion of the  $\text{Ly}\alpha$  nebula is at least  $10''$  in size, but that there is faint diffuse emission extending over larger scales. In order to explore the full spatial extent of the nebula, we compared its radial profile with that of stars measured in the same image. Figure 8 shows the integrated radial profile of the nebula compared with the median profile determined from 10 stars in the NB4448 image, normalized to the same total flux. It is clear that the nebula is spatially extended to a *radius* of at least  $15''$  (nearly 120 kpc)! There are hints that the nebula may be even more extended, but deeper narrow-band imaging observations are necessary to confirm this.

The emission seen in the narrow-band filter is not significantly affected by continuum emission. The Gunn  $G$  filter only spans the wavelength range  $1240\text{--}1460\text{\AA}$  in the rest frame of the system, and therefore excludes the redshifted  $\text{Ly}\alpha$ , C IV and He II line emission from the nebula. This band provides a good measurement of the line-free flux from the region which we can use to estimate (and subtract) the continuum contribution in the NB4448 filter. In an aperture of  $10''$  radius, the continuum contribution is only  $0.225 \times 10^{-15}$  erg  $\text{s}^{-1}$   $\text{cm}^{-2}$  in the NB4448 filter, i.e., only 7% of the total flux. This estimate assumes that the continuum components are due to interlopers and contribute across the entire wavelength region of

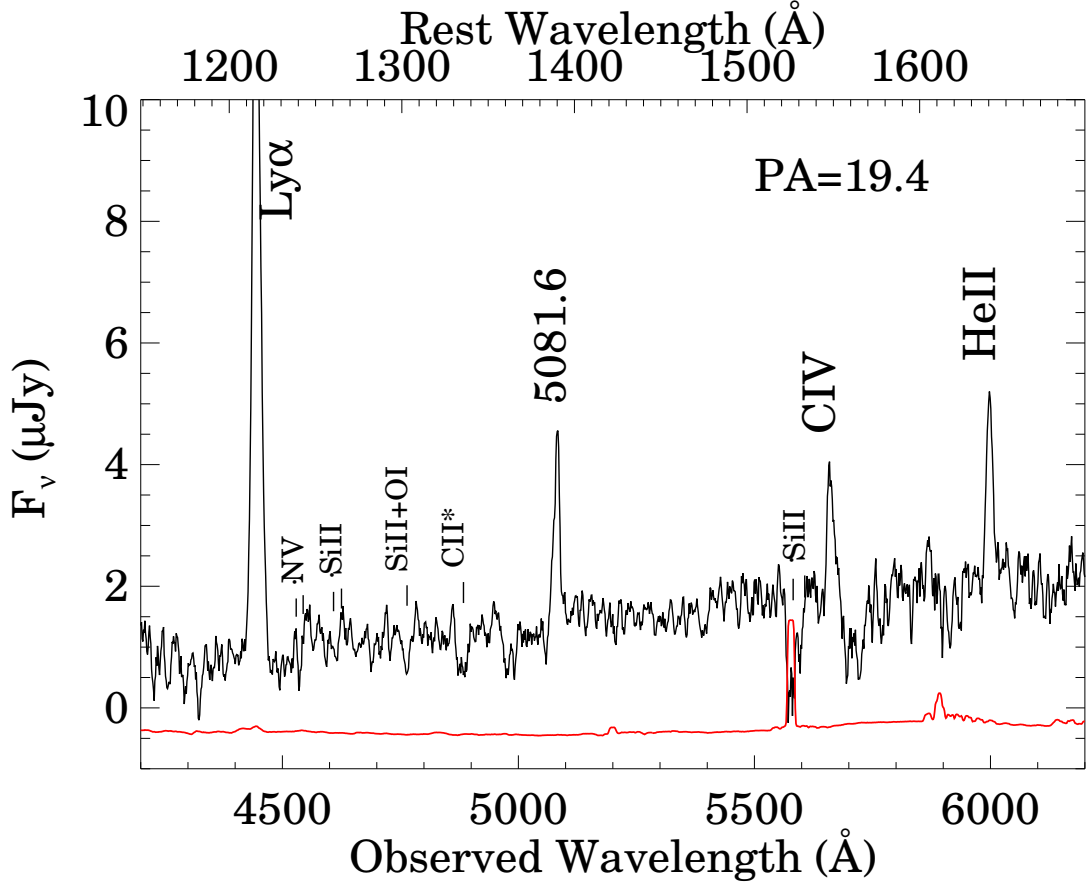


Fig. 4.— One-dimensional spectrum of the Ly $\alpha$  nebula associated with SST24 J1434110+331733 smoothed by 10 $\text{\AA}$ . The aperture is 1''5 wide and 10''9 long and oriented at PA=19.4°. The red line shows the noise spectrum offset by  $-1\mu\text{Jy}$ . The absorption lines arise predominantly from galaxy A, with some contribution from galaxy B noticeable at  $\lambda > 5100\text{\AA}$ . The interloping emission line at  $\lambda=5081.6\text{\AA}$  is only observed in the PA=19.4° observation, and is therefore thought to arise from galaxy B, which lies just to the west of the emission center of the C IV and He II line emission.

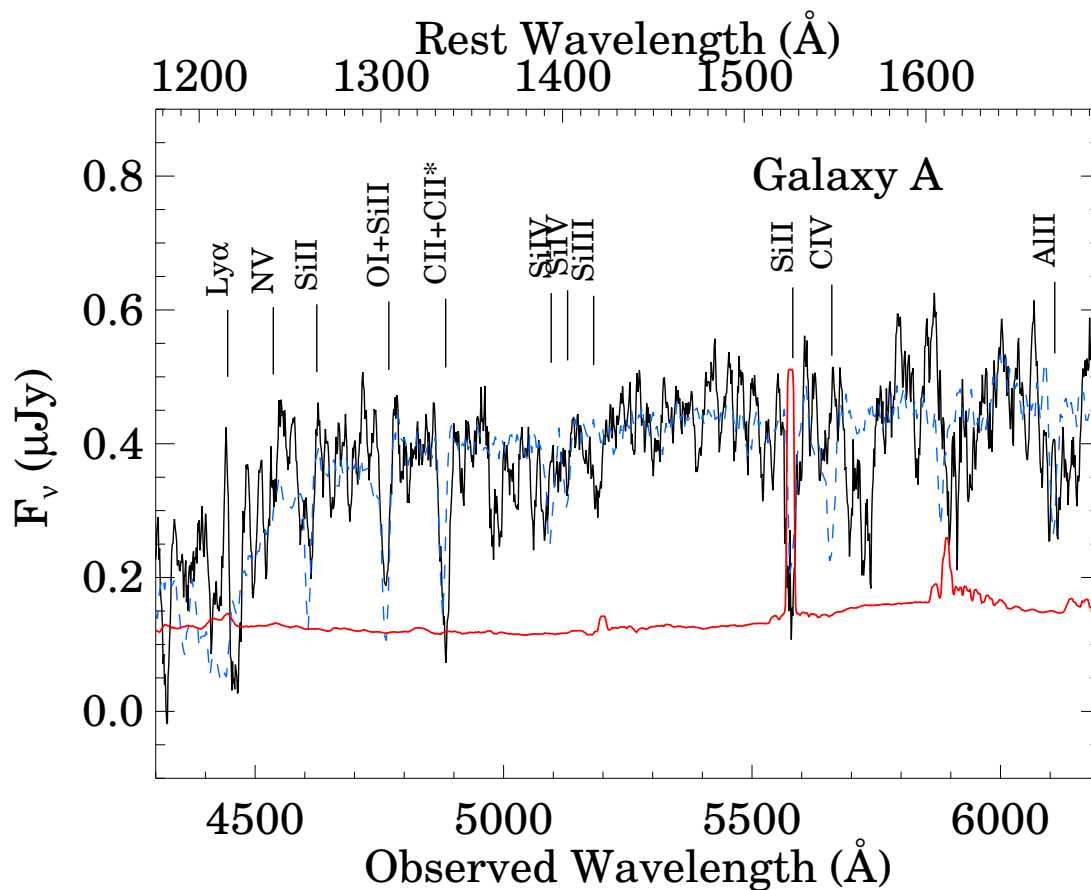


Fig. 5.— One-dimensional spectrum of Galaxy A extracted in an aperture  $1''.5 \times 0''.95$  from the PA=19.4° observation. The dashed line overlaid on the spectrum is the composite spectrum of a  $z \sim 3$  star-forming galaxy constructed from a sample showing strong Ly $\alpha$  absorption (Shapley et al. 2003).

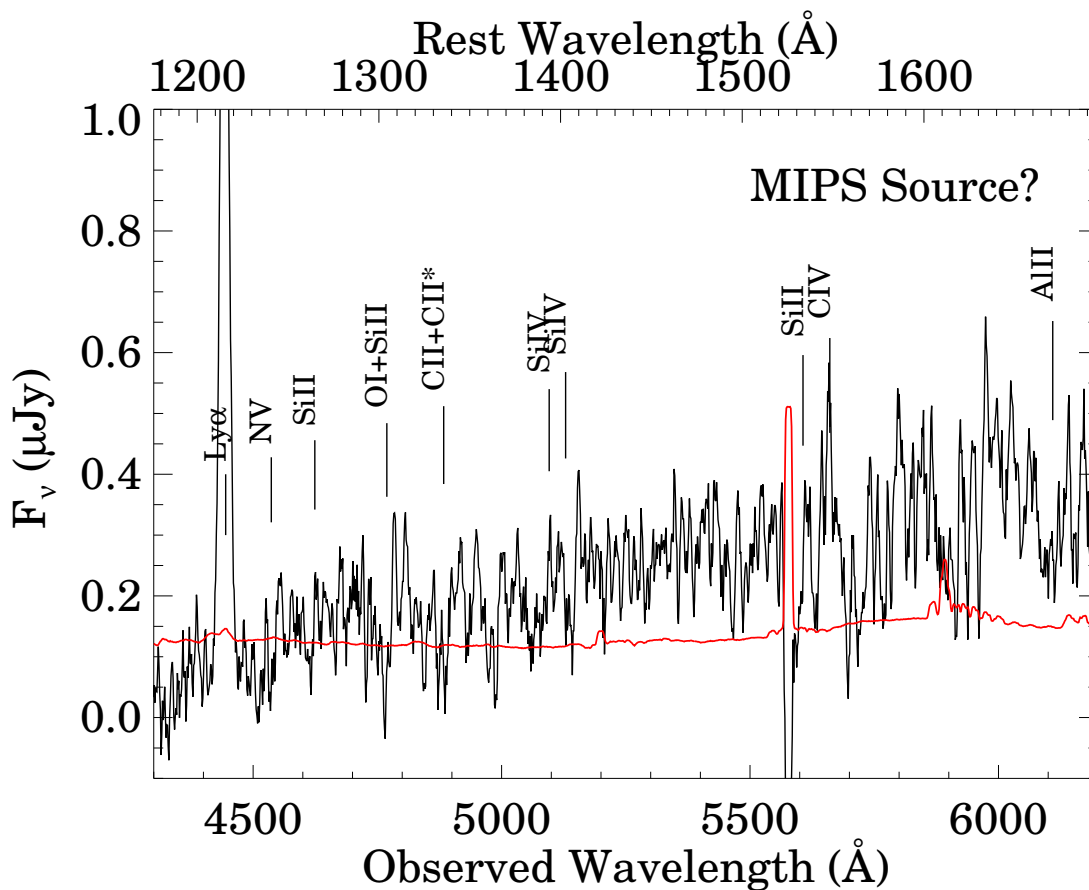


Fig. 6.— One-dimensional spectrum of the continuum object closest to the location of the mid-infrared source. The extraction aperture is  $1''.5 \times 0''.95$  from PA= $19.4^\circ$  observation. The spectrum is much redder than that of galaxy A (figure 5) but shows weak C IV.

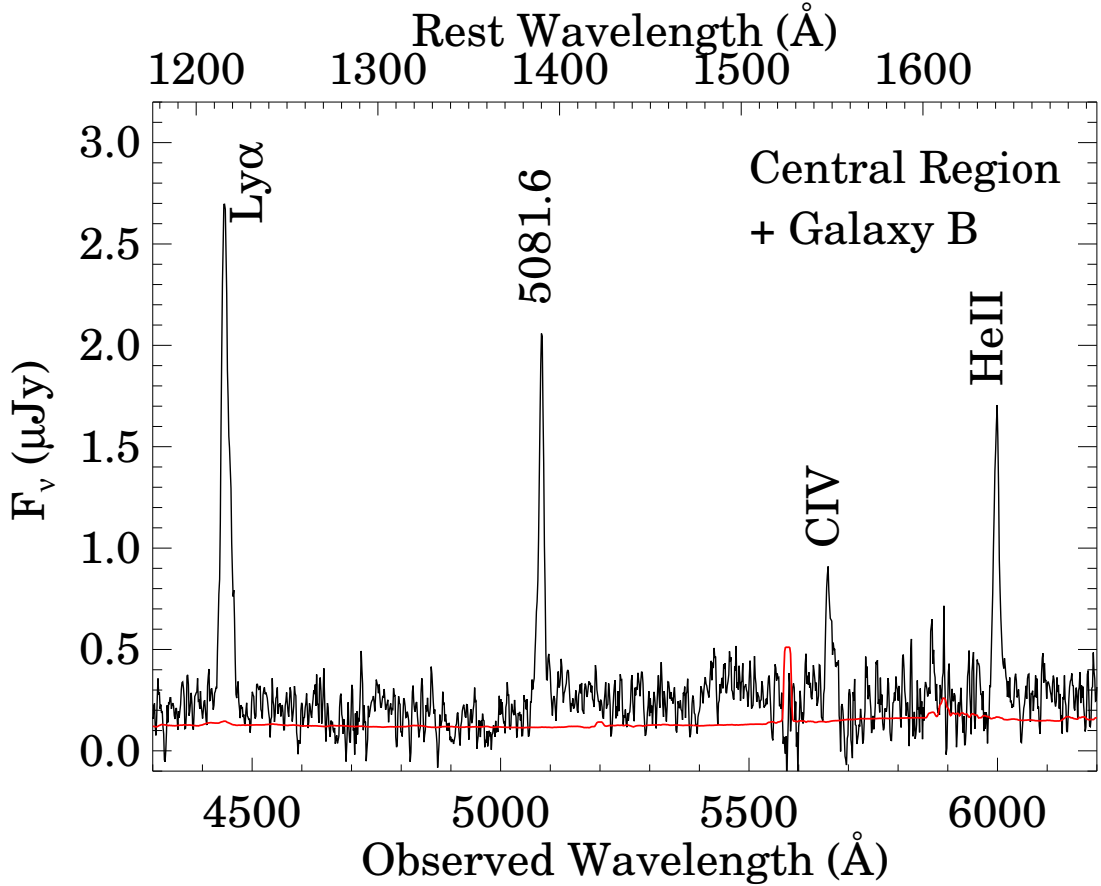


Fig. 7.— One-dimensional spectrum of central region and galaxy B from the PA=19.4° observation. The extraction aperture is  $1''.5 \times 0''.95$ . The spectrum cannot be disentangled cleanly since the two contributing components lie parallel to the dispersion direction, but we suggest that the 5081.6 $\text{\AA}$  line and the continuum emission are dominated by galaxy B, whereas the Ly $\alpha$ , C IV and He II emission arise from the central region of the nebula.

the narrow-band filter. If we instead assume that the continuum arises from sources at the redshift of the nebula, then the continuum contribution within the narrow-band filter would be reduced due to Ly $\alpha$  forest absorption in the intergalactic medium. Using the Madau (1995) approximation for the total continuum absorption, we estimate that the continuum contribution would be about 13% smaller under this assumption, and the total derived Ly $\alpha$  flux imperceptibly larger.

### 3.5. Velocity Structure in the Nebula

Our spectroscopic observations are not sufficiently deep to detect the nebula across its full extent, and we restrict our discussion here to the central 8'' region.

Ly $\alpha$  is a resonance line, and its profile is generally dominated by radiative transfer effects, being affected by resonant scattering and absorption by gas and dust. It is therefore generally a poor tracer of the gravitational potential or the physical properties of the gas. However, at present, this is the only real tracer we have of this system; we therefore use it to provide some indication of the kinematic properties of the system with these caveats in mind.

We extracted spectra in 0''.4 (3-pixel) apertures from each of our spectroscopic observations and fit the Ly $\alpha$  profile with a Gaussian model. The fits are fairly good approximations to the emission line profile; the profiles are only very slightly asymmetric across most of the nebula. We also performed similar fits on the [OI] $\lambda$ 5577 night sky emission line, and found that the tilt this line varied by  $\leq \pm 5$  km s $^{-1}$  across the portion of the slitlets covering the Ly $\alpha$  nebula.

Figure 9 shows the velocity structure in the Ly $\alpha$  line as determined by these fits. The seeing for both observations was typically twice the aperture, and neighboring points in the figure are therefore correlated. The nebula exhibits a monotonic change across the central  $\approx 4''$  in both the central velocity and the velocity dispersion, with deviations from this trend only near the extrema where the signal-to-noise ratio is low.

The remarkable aspect of the measured profile is that its velocity varies so uniformly across the central region. Fitting a straight line to the data from the two observations using a robust least absolute deviation algorithm results in a velocity profile across this central region of  $v = 36.2 - 124.1r$  km s $^{-1}$  in PA=0 $^\circ$  and  $v = 9.7 - 75.5r$  km s $^{-1}$  in PA=19.4 $^\circ$ , where  $r$  is the angular separation in arcseconds. This smooth variation is unlikely to be due to a smooth change in the absorption by neutral hydrogen, since the line profile does not show strong evidence for this. If it is due to the gas kinematics, then the variation could be due

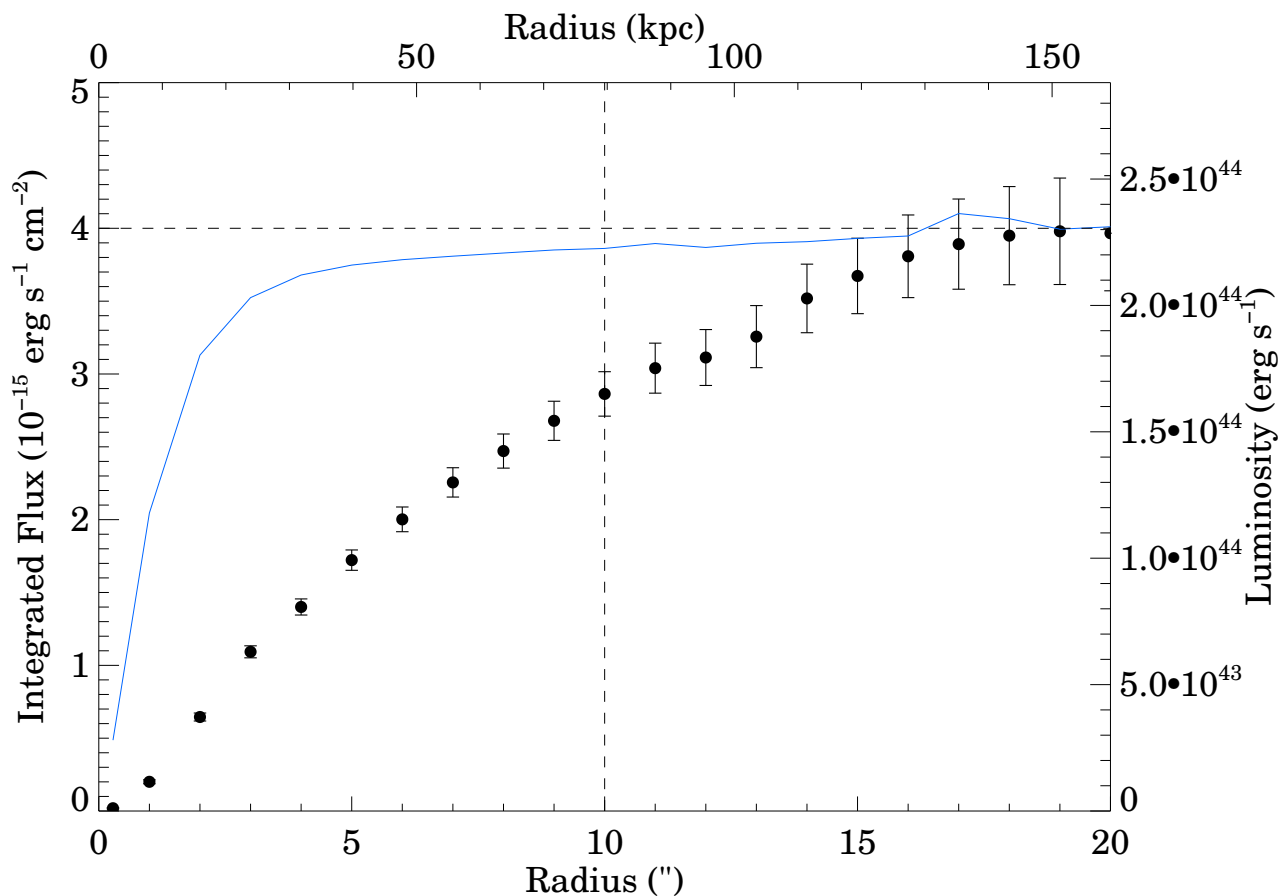


Fig. 8.— The integrated flux of Ly $\alpha$  as a function of radius as measured in the NB4448 image (filled circles). The solid line shows the mean stellar profile in the image, determined using 10 stars. The filled circles represent the integrated Ly $\alpha$  profile after subtraction of the continuum estimated using the Gunn  $G$ -band observations. The dashed vertical line at a radius of 10" denotes our chosen (conservative) aperture size for most of the measurements presented in this paper. The horizontal dashed line is for reference.

to infall, outflow or rotation, and it is not easy to discriminate between these options with the present data.

### 3.6. Spectral Energy Distribution

Figure 10 shows the spectral energy distribution (hereinafter SED) of SST24 J1434110+331733. The optical data points should be regarded as upper limits, since they include continuum contributions from galaxies A and B.

A model for the SED of Arp 220 (constructed from the models of Silva et al. (1998) and Spoon et al. (2004)) placed at  $z = 2.6562$  and scaled by a factor of 26 is shown for comparison in figure 10. The scaling factor was chosen to match the observed IRAC  $8\mu\text{m}$  flux density of SST24 J1434110+331733. The SED of Arp 220 differs from that of SST24 J1434110+331733 in two ways. First, the rest-frame UV emission observed in SST24 J1434110+331733 is much larger than that from Arp 220. This is not surprising: as mentioned before, the UV points are contaminated by other sources (and the bluest point by the strong Ly $\alpha$  line emission). Second, the  $5.8\mu\text{m}$  and  $8.0\mu\text{m}$  IRAC points lie significantly above the prediction of the Arp 220 template. This region of the spectrum is of interest because it is where the SED of Arp 220 transitions from being dominated by starlight at shorter wavelengths to being dominated by dust emission at longer wavelengths. The SED of SST24 J1434110+331733 shows no evidence for such a transition, suggesting that perhaps there is little or no significant contribution from starlight in this portion of the spectrum. Indeed, the mid-infrared continuum measurements from Spitzer ( $3.6\mu\text{m} - 24\mu\text{m}$ ) are well-modeled by a simple quadratic power-law,  $f_\nu \propto \nu^{-2}$ , also suggesting that the Spitzer bands are not strongly affected by emission from polycyclic aromatic hydrocarbons (PAHs), of which the strongest features are redshifted out of the IRAC bandpasses.

The mid-infrared color of SST24 J1434110+331733 lies in the region of parameter space more generally occupied by quasars than by normal star-forming galaxies (e.g., Stern et al. 2005; Lacy et al. 2004). Figure 10 also shows the SED of the Seyfert 1 galaxy Mrk 231 (e.g., Ivison et al. 2004) placed at the redshift of SST24 J1434110+331733 and scaled by a factor of 2. The SED of Mrk 231 is a better fit to the observed  $3.6\mu\text{m}$  to  $24\mu\text{m}$  photometry of SST24 J1434110+331733, and suggests that this source is an enshrouded AGN. The observed excess in the MIPS  $24\mu\text{m}$  band over the Mrk 231 SED may be due to  $7.7\mu\text{m}$  PAH emission.

The most likely emission mechanism responsible for the mid-infrared luminosity is dust emission. Emission at these wavelengths would require dust at warm temperatures ( $\gtrsim 500$  K), higher than those typically seen in normal or ultraluminous star-forming galaxies. How-

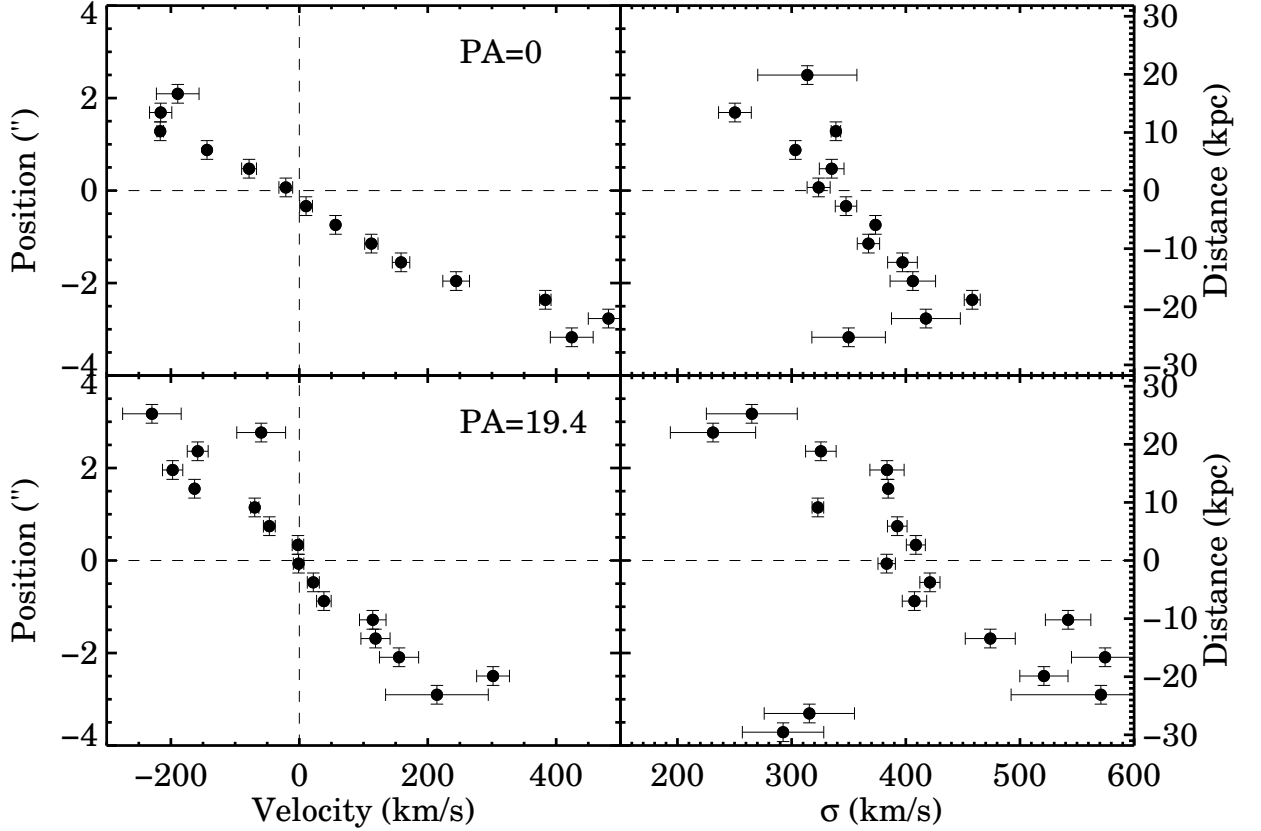


Fig. 9.— Kinematics of the gas in the  $\text{Ly}\alpha$  nebula surrounding SST24 J1434110+331733. The top two panels show the spatial variation in central velocity (left) and velocity dispersion (right) determined from Gaussian fits to the  $\text{Ly}\alpha$  emission line profile measured using the  $\text{PA}=0^\circ$  observation. The lower panels show the measurements from the  $\text{PA}=19.4^\circ$  observation. The origin for the ordinate is defined as the spatial location of the centroid of the  $\text{Ly}\alpha$  emission (i.e., the same as in figure 1). The velocity origin is defined using the wavelength of the  $\text{He II}\lambda 1640$  emission line.

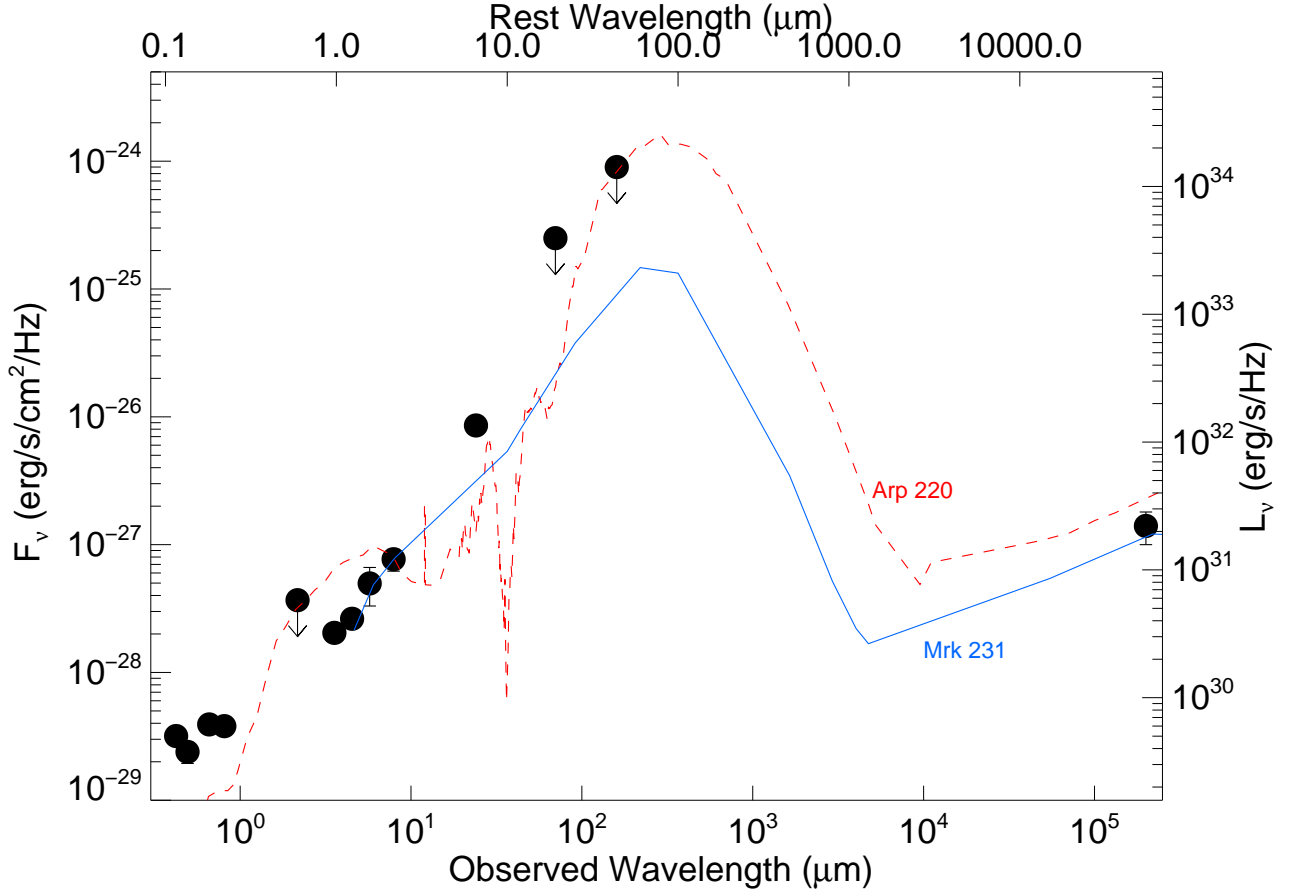


Fig. 10.— The spectral energy distribution of SST24 J1434110+331733. The optical points ( $\lambda_{\text{obs}} < 1\mu\text{m}$ ) should be regarded as upper limits, since they include continuum contributions from galaxies A and B. The red dashed curve is the SED of Arp 220 ( $\lambda < 5\mu\text{m}$  from Spoon et al. (2004) and  $\lambda > 5\mu\text{m}$  from Silva et al. (1998)), scaled in luminosity by a factor of 26, for comparison. Note the discrepancy between the two objects near  $\lambda_{\text{obs}} \approx 10 - 20\mu\text{m}$ , where the SED of Arp 220 transitions from being dominated by starlight to being dominated by dust emission; SST24 J1434110+331733 shows no obvious evidence for such a transition. The blue solid line represents the SED of Mrk 231 from Ivison et al. (2004), scaled by a factor of 2.

ever, a power-law spectrum of  $F_\nu \propto \nu^{-2}$  can also be produced by synchrotron radiation from power-law distribution of electrons, with  $N(E) \propto E^{-5}$ . At longer wavelengths, synchrotron self-absorption sets in and the spectrum should take on a  $\nu^{2.5}$  shape. We can use the faint radio detection of 0.14 mJy and estimate the turnover frequency to be  $\sim 1.2 \times 10^{11}$  Hz (2.5mm). This is not a very useful constraint, especially since a synchrotron spectrum of this sort has never been observed in an extragalactic source. If the slope of the radio spectrum is similar to that of Mrk 231 and its extrapolation to the mid-infrared significantly undershoots the observed mid-infrared flux densities, then the emission mechanism for the mid-infrared is thermal emission from dust grains. Observations in the sub-mm to radio wavelengths will be necessary to better constrain the radiation mechanism for the IR portion of the SED.

If SST24 J1434110+331733 has a similar SED to that of Arp 220 (Mrk 231), the comparison suggests that it has a total far-infrared luminosity of  $L_{\text{IR}} \lesssim 7.5 \times 10^{13} L_\odot$  ( $1.1 \times 10^{13} L_\odot$ )! We emphasize, however, that these estimates are very uncertain at present, since the bulk of the luminosity emerges at wavelengths at which the flux density of SST24 J1434110+331733 is currently unknown and require a large bolometric correction. Measurements at sub-mm wavelengths are clearly crucial to establishing the shape of the SED near its peak and providing a better measure of the bolometric luminosity. If the SED is similar to that of Arp 220 (Mrk 231), we would expect 450 $\mu\text{m}$  and 850 $\mu\text{m}$  flux densities of  $\lesssim 120$  mJy (8 mJy) and  $\lesssim 40$  mJy (2 mJy) respectively. Clearly, these predictions are all within the reach of the current sub-mm observations.

We note that the mid-infrared-to-radio flux density ratio observed in SST24 J1434110+331733,  $q_{24} \equiv \log[f_\nu(24\mu\text{m})/f_\nu(20\text{cm})] \approx 0.8$ , shows remarkable similarity to that of starburst galaxies, which typically have  $q_{24} \equiv \log[f_\nu(24\mu\text{m})/f_\nu(20\text{cm})] = 0.84 \pm 0.28$  (Appleton et al. 2004). Mrk 231 also falls on this relation, although it is an obscured Seyfert 1; this is because its mid-infrared and radio emission are dominated by flux from the circumnuclear starburst rather than the active nucleus.

#### 4. Discussion

In the previous section, we presented our various observations of SST24 J1434110+331733. Here, we discuss the implications of our observations for understanding the physical nature of this remarkable system.

Large Ly $\alpha$  nebulae such as SST24 J1434110+331733 are rare. Thus far, most known large Ly $\alpha$  nebulae are associated with powerful radio galaxies (e.g., McCarthy et al. 1990; van Ojik et al. 1997; Pentericci et al. 1997; Dey et al. 1997; Dey 1999; Villar-Martín et al.

2002, 2003; Reuland et al. 2003). Among radio quiet sources, there are two similarly large nebulae at  $z \approx 3.09$  ( $\text{Ly}\alpha$  “blobs” LAB1 and LAB2; Steidel et al. 2000) and one at  $z \approx 2.38$  (2142–4420 B1; Francis et al. 1996). These latter systems are associated with large galaxy overdensities, and follow-up deeper  $\text{Ly}\alpha$  imaging of these regions has resulted in the discovery of numerous other smaller  $\text{Ly}\alpha$ -emitting nebulae (e.g., Palunas et al. 2004; Matsuda et al. 2004). Similar overdensities have also been found associated with some of the  $\text{Ly}\alpha$  nebulae associated with radio sources (e.g., Keel et al. 1999; Pentericci et al. 2000).

The rarity of these  $>100$  kpc  $\text{Ly}\alpha$  clouds, their association with powerful AGN and galaxy overdensities, and their energetics, all suggest that these regions are the formation sites of the most massive galaxies. If so, understanding the physical conditions and energetics of these systems can provide important insights into the massive galaxy formation process.

At present, it is still not clear what powers the nebulae. Is the  $\text{Ly}\alpha$  emission cooling radiation of infalling, shocked, pristine gas (Haiman et al. 2000)? Or is it photoionized by hot stars or AGN (e.g., Haiman & Rees 2001)? Or is it the cooling of outflowing shocked gas (cf. the “superwind model” of Taniguchi & Shioya 2000; Francis et al. 2001)? Much of the recent literature on the extended  $\text{Ly}\alpha$  nebulae has focussed on the radio-quiet systems (LAB1, LAB2 and the sources at  $z = 2.38$ ), perhaps because the absence of an obvious radio source suggested an absence of AGN (and their associated complexity) in these systems. However, more recent observations of the LAB1 system now find that it may also contain buried AGN (Chapman et al. 2004). Moreover, there are many similarities between the outer, kinematically quieter regions of the  $\text{Ly}\alpha$  halos surrounding the powerful radio sources and the radio quiet “blobs”. All this suggests that AGN may exist in all these nebulae: after all, if all massive bulges host massive black holes, then perhaps the formation of the active nucleus accompanies the formation of the galaxy.

It is then perhaps not surprising that the known large  $\text{Ly}\alpha$  nebulae reveal such complexity: compact obscured regions, formed galaxies, revealed AGN, all within their extent. If these are the largest protogalactic regions, one might expect that both star- and AGN-formation could proceed within the cloud.

#### 4.1. Mass of the Nebula

The total mass of the nebula can be estimated dynamically (from the velocity profile of the  $\text{Ly}\alpha$  line), under the relatively poor assumptions that the line profile is not significantly affected by absorption and scattering. The smooth variation of the central wavelength of the line, the relatively constant velocity dispersion, and the overall symmetry of the line

all provide some justification to these assumptions. If the velocity profile observed in the inner regions is primarily the result of rotation, then the mass internal to a radius  $r = 4''$  ( $\approx 32 \text{ kpc}$ ) is  $M(r \leq 4'') \approx 0.6 - 1.6 \times 10^{12} \sin^{-2}i M_{\odot}$ , where the large range is due to the range in the velocity profile fits measured from the two different spectroscopic observations. The velocity profile is not well measured at radii larger than  $\sim 30 \text{ kpc}$ .

Interpreting the line width is also fraught with uncertainty. Absorption by neutral hydrogen would result in the measured width being an underestimate of the true width; whereas resonant scattering would likely broaden the line. The velocity dispersion of  $\approx 400 \text{ km s}^{-1}$  is too large to be due to the thermal motions of the gas. If it is, instead, due to the random motions of clouds within the nebula, then we can estimate the dynamical mass of the nebula to be  $M(r \leq 4'') \approx 6 \times 10^{12} M_{\odot}$ . These dynamical mass estimates derived from the line centroid and width are very large. However, they are surprisingly similar to the estimates derived for the large Ly $\alpha$  halos around high-redshift radio galaxies, where dynamical mass estimates range from  $0.3 - 10 \times 10^{12} M_{\odot}$  (Reuland et al. 2003; Villar-Martín et al. 2003; van Ojik et al. 1997). We note that in general such dynamical estimates are more sensitive to larger masses, since lower mass systems will have gradients that are not resolved by typical faint-object spectroscopic observations.

A separate estimate of the ionized gas mass may be derived by estimating the electron density  $n_e$  from the net luminosity of the Ly $\alpha$  emission line (cf. McCarthy et al. 1990),  $M_{\text{ion}} = 1.25m_p n_e f_V V \approx 1.7 \times 10^{12} f_V^{0.5} (n_e f_V^{0.5} / 0.026 \text{ cm}^{-3}) M_{\odot}$ . The filling factor  $f_V$  is unconstrained by the present data, but observations of line-emitting regions in cluster cooling flows suggest filling factors of order  $10^{-5}$  to  $10^{-6}$  (e.g., Heckman et al. 1989), which would suggest ionized gas masses of  $M_{\text{ion}} \approx 1.7 \times 10^9 (f_V / 10^{-6}) M_{\odot}$ . If  $\Omega_b = 0.04$  and  $\Omega_{\text{matter}} = 0.30$ , then a comparison with the dynamical mass estimates suggest ionization fractions of  $\lesssim 0.013 (f_V / 10^{-6})^{0.5} (10^{12} / M_{\text{tot}})$ , and a rough upper limit to the filling factor of  $\sim 7.7 \times 10^{-5}$ . The ionized gas fraction is low for a typical hot plasma, suggesting that a significant fraction of the mass might be contained in colder (neutral), collapsed objects, e.g., the galaxies that are forming within the cloud. Although this argument is only speculative at present, better measures of the gas density, temperature and filling factor, perhaps from deep rest-frame optical spectroscopy, can help constrain the relative fractions of hot and cold gas.

## 4.2. Physical State of the Gas and the Nature of the Ionizing Source

It is difficult to place firm constraints on the temperature of the gas cloud since at present Ly $\alpha$  is the only emission line that we detect across the spatial extent of the nebula;

He II $\lambda$ 1640, C IV $\lambda\lambda$ 1550 and C III] $\lambda$ 1909 are only detected in a localized region near the center of the nebula, and in addition, C IV and C III] are observed in a red, optically visible continuum source which may be associated with the mid-infrared source. There is also weak evidence that C IV may be spatially extended between the central region and the MIPS source.

The line ratios of the gas in the central region are not representative of shock ionization: the shock models of Dopita & Sutherland (1996) typically produce much higher C IV $\lambda\lambda$ 1550/He II $\lambda$ 1640 ratios (e.g.,  $\sim 2 - 20$  for shock velocities  $v_{\text{shock}} \sim 500 - 150 \text{ km s}^{-1}$ ) as compared to the observed value of C IV/He II and tend to overproduce NV $\lambda$ 1240 relative to what is observed in this source. Higher shock velocities ( $v_{\text{shock}} > 500 \text{ km s}^{-1}$ ), where better matches might be produced, are unlikely given the low velocity widths observed for the C IV and He II emission lines. We cannot yet, however, rule out shock ionization in other regions of the nebula where Ly $\alpha$  is the only detected emission line.

The He II $\lambda$ 1640 emission line is unusually strong in the central region. Its strength may be indicative of low metallicity (and therefore high temperatures) in the ionized gas in this region. However, models of star-forming galaxies typically only show He II with rest-frame equivalent widths of  $\gtrsim 15 \text{ \AA}$  at very low metallicities ( $Z \lesssim 10^{-7}$ ) and at very young ages  $\lesssim 2 \text{ Myr}$  (Schaerer 2003). Although it is possible we are witnessing this object at such an unusual and early epoch, it would be very improbable; it is therefore unlikely that the strong He II is due to low metallicity gas.

Harder ionizing continua, such as those generated by AGN, can also produce strong He II; indeed, comparable strengths of C IV and He II are commonly observed in radio galaxy spectra and “type 2 quasars” and are generally attributed to photoionization by a power-law continuum. The one oddity is the relative weakness of the observed C III] emission: most radio galaxy spectra show C III]/C IV  $\sim 1$ , whereas we observe a ratio in this system of  $\approx 0.2$ . The observed ratio can however be produced by a power-law ionizing spectrum and is characteristic of a large ionization parameter  $U \equiv Q(\text{H})/4\pi R^2 n_e c \sim 10^{-2}$  for a  $f_\nu \propto \nu^{-1}$  continuum (Ferland 1981) in this central region.

A crude constraint on the slope of the ionizing spectrum can be derived from the ratio  $\eta$  of the number of He<sup>+</sup> ionizing photons ( $\approx 3.7 \times 10^{53} \text{ s}^{-1}$ ) relative to the number of H ionizing photons ( $\approx 1.6 \times 10^{55} \text{ s}^{-1}$ ):  $\eta \equiv Q(\text{He}^+)/Q(\text{H}) = 0.023$  (for a  $T = 10^4 \text{ K}$  gas) (e.g., Schaerer 2002). If we relate this ratio to the number of photons at 54 eV relative to that at 13.6 eV, this ratio suggests a spectral shape of  $F_\nu \propto \nu^{-2.7}$ . It is intriguing that this slope is even steeper than the  $F_\nu \propto \nu^{-2}$  spectrum derived by extrapolation of the mid-infrared SED. We have not accounted for Ly $\alpha$  absorption in this estimate, which would suggest that the ionizing spectrum is even steeper, i.e.,  $\alpha < -2.7$ . Note that here we have compared the full

10'' radius aperture measurement of Ly $\alpha$  with the spectroscopic measurement of He II $\lambda$ 1640. If we compare just the measurements in the same spectroscopic apertures, we derive a ratio of  $\eta = 0.21$  for  $T = 10^4$  K, which would suggest an extremely hard ionizing spectrum of  $F_\nu \propto \nu^{-0.116}$ . This latter estimate is unlikely to be realistic, since the H $^+$  ionization zone is likely to extend over a much larger scale than the He $^{++}$  zone, but we can take it to be a very firm upper limit for the slope of the ionizing continuum.

If we assume normal HII region electron temperatures of  $T_e \sim 10^4$  K in the central region, then we can estimate the electron density using the strength of the Ly $\alpha$  emission in the same aperture used to measure the high ionization lines (see Table 2). The Ly $\alpha$  luminosity is given as  $L_{\text{Ly}\alpha} = (j_{\text{Ly}\alpha}/j_{\text{H}\beta})n_e n_p f_V V h\nu_{\text{H}\beta} \alpha_{\text{H}\beta}^{\text{eff}} \approx 4.05 \times 10^{-24} n_e^2 f_V V$ , where  $V$  is the volume of the emitting region,  $n_e$  and  $n_p$  are the electron and proton number densities,  $f_V$  is the filling factor of the ionized gas, and  $\alpha_{\text{H}\beta}^{\text{eff}}$  is the effective recombination coefficient for H $\beta$  (Storey & Hummer 1995). In the central region, we find  $n_e f_V^{0.5} \approx 0.25 \text{ cm}^{-3}$ ; combined with the ionization parameter estimate, this implies a hydrogen ionizing photon flux in the central region of  $Q(\text{H}) \approx 3 \times 10^{54} f_V^{-0.5} \text{ s}^{-1}$  photons  $\text{s}^{-1}$ . We have no direct measure of the electron density, and therefore no firm constraints on the volume filling factor of the ionized gas. However, if we use the rough upper limit to the filling factor from the previous subsection, then  $Q(\text{H}) \gtrsim 6 \times 10^{56}$  photons  $\text{s}^{-1}$ .

Using a similar analysis for the total Ly $\alpha$  luminosity measured in a 10'' radius aperture, we find  $n_e f_V^{0.5} \approx 0.026 \text{ cm}^{-3}$  for the average density in the nebula as a whole. For values of the filling factor  $10^{-3} > f_V > 10^{-6}$ , the average electron density in the line-emitting regions is in the range  $0.8 < n_e < 26 \text{ cm}^{-3}$ .

### 4.3. Energetics

The Ly $\alpha$  luminosity of the nebula within a 10'' radius aperture is  $\approx 1.67 \times 10^{44} \text{ erg s}^{-1}$ . This is comparable to the luminosities of the other well-known Ly $\alpha$  nebulosities, LAB1 (Steidel et al. 2000,  $1.4 \times 10^{44}$ ) and 2142–4420 B1 (Francis et al. 2001; Palunas et al. 2004,  $\approx 8 \times 10^{43} \text{ erg s}^{-1}$ ). If it is due to young, hot stars distributed over the face of the nebula in a very extended star-forming region, then the luminosity implies a net star-formation rate  $SFR_{\text{Ly}\alpha} = L_{\text{Ly}\alpha}/(1.12 \times 10^{42} \text{ erg s}^{-1}) \approx 150 M_\odot \text{ yr}^{-1}$  (Kennicutt 1983).

It is not clear what source(s) power the Ly $\alpha$  emission. No obvious single compact source with high UV luminosity is visible within the extent of the nebula. The two galaxies A and B do not appear to be plausible candidates for the sources of the photoionizing radiation: galaxy B is at the wrong redshift, and galaxy A does not show any strong Ly $\alpha$  emission

associated with it and its UV luminosity at  $\lambda_{\text{rest}} = 1500\text{\AA}$  only corresponds to a modest star-formation rate of  $SFR_{\text{UV}} = L_{\text{UV}}/8 \times 10^{27} \text{ erg s}^{-1} \text{ Hz}^{-1} \approx 8 M_{\odot} \text{ yr}^{-1}$  (e.g., Madau et al. 1998).

It is also not clear if the MIPS source is the source of the photoionizing radiation: it is faint at rest-frame UV wavelengths and its mid-infrared emission suggests that the source, although very luminous, is almost completely obscured from view by dust. It is therefore unlikely that short wavelength ionizing photons could escape from the nebula - clearly, little or no Ly $\alpha$  emission does. Nevertheless, it is intriguing that the estimated far-infrared luminosity of the MIPS source is roughly two and a half orders of magnitude larger than the Ly $\alpha$  luminosity of the entire nebula, and it is possible that some ionizing radiation could leak out in directions other than our direct line of sight. We discuss this further below.

It therefore appears that the Ly $\alpha$  emission is powered by sources hidden from direct view, perhaps partly by the mid-infrared source, perhaps partly by another obscured or mis-directed source lying near the center of the nebula where we also observe the C IV and He II emission lines, or by distributed, faint, ionizing sources, or by shocks associated with the infall of gas into the region. The dynamical timescale of the nebula is given by  $t_{\text{dyn}} \approx \frac{\pi}{2} \sqrt{R^3/2GM} \approx 0.37 \text{ Gyr}$ . This is much smaller than the age of the Universe at  $z = 2.656$  (2.4 Gyr in our adopted cosmology), and suggests that we are witnessing the nebula in a young phase. The temperature of the nebular gas is unknown, but if we assume a temperature of  $10^4 \text{ K}$ , then the cooling timescale is  $t_{\text{cool}} \approx \frac{3\rho kT}{2\mu\Lambda(T)} \approx 2.07 \times 10^{11} \text{ s} (T/10^4\text{K}) (n_e/1\text{cm}^{-3})^{-1} (\Lambda(T)/10^{-23} \text{ erg cm}^3 \text{ s}^{-1})^{-1}$  (Padmanabhan 2002; Sutherland & Dopita 1993). For gas between  $10^4 - 10^5$ ,  $\log(\Lambda(T))$  can vary from  $-23.4$  to  $-21.0$  depending on the exact temperature and metallicity, suggesting cooling times which are very short ( $t_{\text{cool}} \lesssim 1.6 \times 10^4 \text{ year}$ ), implying that some source of energy (shocks? ionizing photons?) is required to maintain the nebula and render it visible. Taken at face value, the large ratio of  $t_{\text{dyn}}/t_{\text{cool}}$  would imply rapid collapse of the cloud into star-forming clumps.

#### 4.4. The Mid-Infrared Source

The source SST24 J1434110+331733 detected in the *Spitzer* IRAC and MIPS bands lies within the extent of the Ly $\alpha$  nebula, roughly 2.5 (20 kpc) away from the center. The optical spectra show a faint continuum source within the MIPS error circle, just to the southeast of the MIPS position. The spectrum of this source appears to be significantly redder than galaxy A ( $F_{\lambda} \propto \lambda^{0.075 \pm 0.006}$  for the MIPS source in the observed optical regime, versus  $F_{\lambda} \propto \lambda^{-0.076 \pm 0.004}$  for Galaxy A), but it does show weak associated C III] emission and possibly some C IV emission certifying its association with the Ly $\alpha$  nebula. The optical

spectrum shows no obvious signs of AGN activity (e.g., broad emission lines or strong high-ionization lines), but instead shows possible absorption lines similar to those observed in young, star-forming Lyman-break galaxies.

A fit to the SED in the *Spitzer* bands suggests a power-law spectrum of the form  $L_\nu \approx 2.7 \times 10^{31} (\nu/10^{14} \text{Hz})^{-2} \text{ erg s}^{-1} \text{ Hz}^{-1}$  (figure 11). Rather surprisingly, extrapolating this power-law to rest-frame UV wavelengths 1300–1800Å is consistent with the observed spectrum of the faint optical source believed to be associated with the MIPS source, only overshooting the observed spectrum by a factor of  $\sim 1.3$ – $1.7$  (figure 11). This offset is perhaps not surprising, given that we are comparing the large aperture total flux densities of the *Spitzer* data with the small aperture ( $1.5'' \times 1.0''$ ) spectral extraction.

The mid-infrared source has poorly constrained flux densities at long wavelengths ( $\gtrsim 100 \mu\text{m}$ ) where much of its luminosity likely emerges. As discussed in section § 3.6, if the SED is similar to that of known ULIRGs, the far-infrared luminosity of the source is likely to be in the range  $1 - 5 \times 10^{13} L_\odot$ . If this object is a starburst, this luminosity corresponds to a star-formation rate  $SFR_{\text{IR}} \approx 1700 (L_{\text{IR}}/10^{13} L_\odot) M_\odot \text{ yr}^{-1}$ . If its luminosity-to-mass ratio is comparable to ULIRGs (i.e.,  $L/M \sim 100 - 200$ ), the prodigious luminosity implies a total mass in dust of about  $M_{\text{dust}} \sim 0.2 - 5 \times 10^9 M_\odot$  if  $M_{\text{dust}}/M_{\text{gas}} = 0.01$ . These estimates are very coarse, but it is clear that these large bolometric luminosities imply very large masses of dust, and that a substantial mass of baryons has already been cycled through stars to produce this mass of dust.

Although the mid-infrared source is extremely energetic and lies within the nebula, it is not clear whether it is responsible for photoionizing the nebula. If we assume that the  $\nu^{-2}$  power-law represents the intrinsic spectrum of the mid-infrared source, and if it can be extrapolated to shorter wavelengths, then we can investigate whether the ionizing photons emitted by this source are sufficient to photoionize the nebula and produce the observed Ly $\alpha$  radiation. Extrapolating the power-law would result in  $\approx 1.8 \times 10^{54}$  ionizing photons between 200Å and 912Å. The luminosity of the Ly $\alpha$  nebula requires  $\approx 10^{55}$  ionizing photons. The MIPS source can therefore be responsible for at most 18% of the Ly $\alpha$  luminosity. This is likely a very strong upper limit, since in reality the rest-frame UV spectrum is observed to be redder than the extrapolation, and our estimate here does not account for any absorption by dust. It is possible, of course, that although the extinction to the source is severe along our line of sight, it may still have low optical depth toward the nebula (say, a mis-directed quasar). Although plausible, the geometry of the source, taken at face value, does not favor such an explanation: the MIPS source is not located at the center of the nebula and instead lies  $\approx 20$  kpc away from the peak of the Ly $\alpha$  emission. The symmetry of the Ly $\alpha$  emission around this peak, the presence of a possible ionizing source near this peak as witnessed by

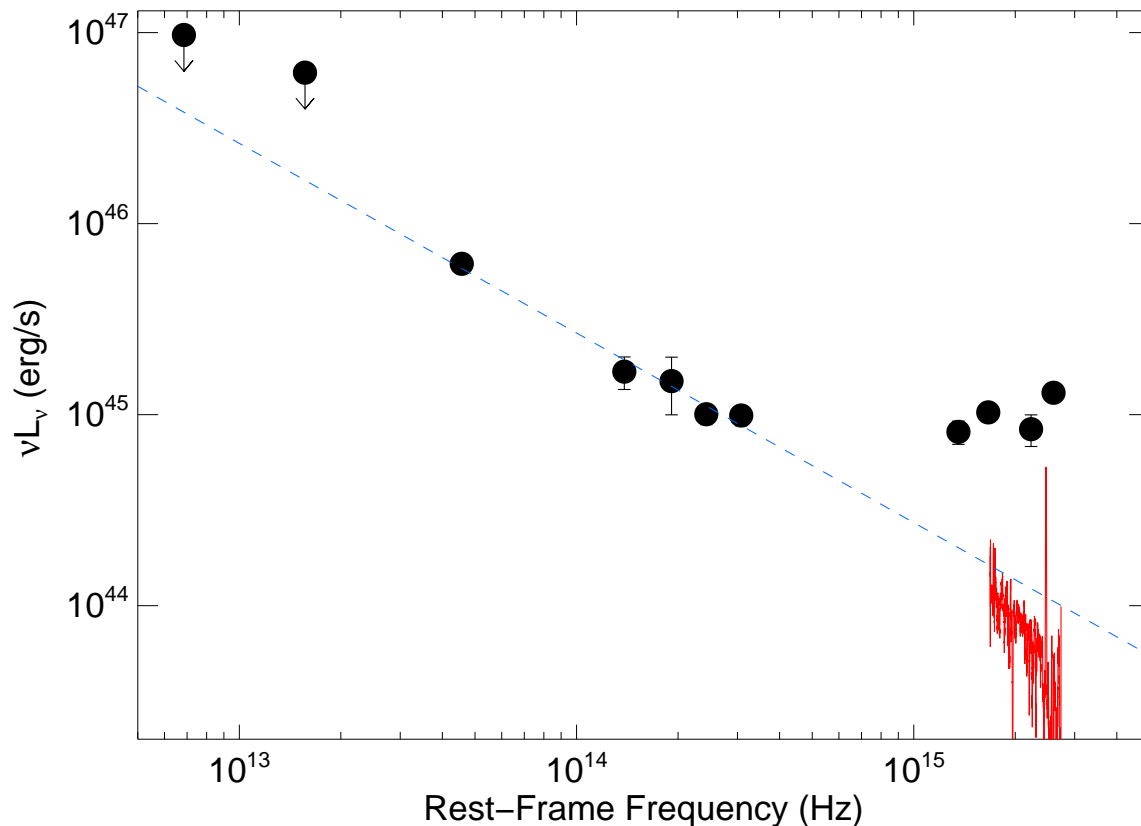


Fig. 11.— The spectral energy distribution of SST24 J1434110+331733, shown here as  $\nu L_\nu$  vs  $\nu$ . The rest-frame UV points ( $\nu > 10^{15}$  Hz) should be regarded as upper limits, since they include continuum contributions from galaxies A and B. The red line at high frequency is the spectrum of the optical continuum source closest to the location of the MIPS source (shown also in figure 6). The dashed blue line is a fit to the *Spitzer* data points,  $L_\nu \propto \nu^{-2}$ .

the presence of He II, C IV and C III] emission, and the lack of strong Ly $\alpha$  emission cospatial with the location of the MIPS source all suggest that it is not primarily responsible for the nebula. Further spectroscopy and high spatial resolution imaging of the cloud are necessary to carefully account for all the possible ionizing sources within the cloud.

The power-law SED in the optical and mid-infrared bands exhibited by SST24 J1434110+331733 and its extreme luminosity are more typical of active galaxies and quasars than of star-forming galaxies (Pier & Krolik 1992; Nenkova et al. 2002, e.g.). It is therefore likely that the infrared luminosity of this source is dominated by an enshrouded AGN, rather than a vigorous starburst; starlight from young stars only begins to dominate the flux at rest-frame UV wavelengths. In this respect, SST24 J1434110+331733 may be very similar to the dust enshrouded systems with extreme 24 $\mu$ m-to-optical colors discovered by Houck et al. (2005). *Spitzer* IRS spectroscopy of these extreme systems has established that they are obscured, dust-enshrouded AGN at  $z \sim 2.5$  with far-infrared luminosities in the range  $6 \times 10^{12-13} L_{\odot}$  (Houck et al. 2005). We speculate that these objects are all extremely massive galaxies caught in an early phase of their formation. Since the AGN is currently dominating the SED, it is tempting to speculate that the supermassive black hole in these extremely massive systems form contemporaneously with the assembly of the galaxy, rather than grow slowly by subsequent accretion.

#### 4.5. Galaxy and AGN Formation in the Cloud

In a seminal work, Elmegreen & Lada (1977) proposed that star formation in molecular clouds in our Galaxy proceeds through the sequential formation of OB subgroups, with each new subgroup driving ionization and shock fronts deeper into the parent molecular cloud, stimulating further star formation. Their model was inspired by observations of a few Galactic star-forming regions (e.g., W3, M 17 and M 42), where this sequence of events can be observed directly: an expanding HII region associated with an OB association located at the edge of a molecular cloud. A host of infrared-luminous cores and maser sources lying within the molecular cloud and near this edge bear witness to active, ongoing star-formation occurring near the location of the shock front, and suggest that the star-formation “front” is slowly eating into the cloud.

It is rather remarkable that the system reported here shows many analogous features: a Lyman break star-forming galaxy, which lies just north of a dust-enshrouded active region, which lies just north of a large region characterized by Ly $\alpha$  cooling radiation. By analogy to the M 17 region, we postulate that this is a time sequence, with the Lyman break galaxy representing the ‘old’, revealed objects, the mid-infrared source representing the site

of current star- and AGN-formation, and the central source and Ly $\alpha$  nebula representing the region where galaxy formation is just beginning. In such an evolutionary scenario, a gas cloud, observed by its cooling radiation, would undergo collapse leading to an initial burst of star-formation and AGN activity. This immediately enshrouds the active region (through the production of dust in the ejecta of first generation supernovae), and then finally leads to a stage when the formed, star-forming galaxy is unveiled. Although highly speculative, this scenario would certainly have many merits. It might explain the low stellar masses observed in the Ly $\alpha$ -bright regions found in the narrow-band surveys (these are the youngest objects that have just started forming stars), the very high star-formation rates observed in the SCUBA galaxies (these represent the peak star-formation phase), the relatively low star-formation rates seen in the Lyman-break galaxies (the early post-starburst phase), and no obvious evidence of systems with intermediate metallicities (they are rapidly enshrouded).

In this case, however, it is very unlikely that the formation events could be triggered by an ionization front: over the several kpc scales in question, the only relevant force is gravity, and the hypothesis presented here is simply that we may be able to estimate the time for the collapse of such a large cloud into its star-forming sub-units by age-dating the various sub-units. If, for example, galaxy A is typical of most Lyman-break galaxies at  $2 < z < 3$ , then we can assume a minimum age of  $\sim 100$  Myr since its last major epoch of star-formation (e.g., Papovich et al. 2001). Since its distance from the center of the Ly $\alpha$  emission is  $\approx 30$  kpc, a naive estimate of the rate at which galaxy formation is proceeding through the region is  $\sim 300$  kpc Gyr $^{-1}$ . Better constraints may be derived by detailed age-dating of the galaxies in the nebula. Our present data preclude such an analysis, but future spectroscopic and multiwavelength imaging observations may allow us to date the various components more reliably.

One timescale of relevance here is the formation time of the AGN associated with the mid-infrared source. Under the assumption that the bulk of the far-IR luminosity is produced by accretion onto a super-massive black hole (SMBH) at the Eddington rate, we estimate a central black hole mass of  $M_{\text{BH}} \approx 2.5 \times 10^8 (L_{\text{IR}}/10^{46} \text{erg s}^{-1}) M_{\odot}$  and an accretion rate of  $\dot{M} \approx 7.6 (L_{\text{IR}}/10^{46} \text{erg s}^{-1}) (0.1/\eta) M_{\odot} \text{ yr}^{-1}$ , where  $\eta$  is the radiative efficiency of the SMBH. If the black hole grows at a constant efficiency, then a  $10^9 M_{\odot}$  SMBH can be created by steady accretion from a small seed  $10 M_{\odot}$  black hole in about  $8 \times 10^8$  years, i.e., a seed formation redshift of  $z \approx 4$ . Our estimates are upper limits for  $M_{\text{BH}}$  and the total growth time. For more massive seeds or merging of multiple seeds during the formation process, the formation time could be significantly shorter (cf. Haiman 2004; Yoo & Miralda-Escudé 2004; Shapiro 2005).

## 5. Conclusions

We have discovered a very large Ly $\alpha$ -emitting nebula at a redshift of  $z = 2.656$ . This is the first such object discovered by its associated  $24\mu\text{m}$  emission. The luminosity of the nebula ( $L_{\text{Ly}\alpha} \approx 1.67 \times 10^{44} \text{ erg s}^{-1}$  within a  $10''$  radius aperture), its large spatial extent ( $> 100 \text{ kpc}$ ), the detection of a star-forming “Lyman-break” galaxy and a source of intense mid-infrared emission within the nebula all suggest that it is the site of massive galaxy formation. In many of these respects, SST24 J1434110+331733 is similar to the Ly $\alpha$  “blob” LAB1 discovered by Steidel et al. (2000). By analogy to the other large Ly $\alpha$  “blobs” known, it is probable that this one sits within a large (several Mpc - scale) structure; further deep, wide-field Ly $\alpha$  imaging of the region should prove fruitful.

Spectroscopy of the Ly $\alpha$  emission reveals that the cloud is kinematically ‘quiet’ at least in its inner regions, showing a slowly and monotonically varying velocity centroid with position and roughly uniform velocity dispersion across its face. If interpreted as rotation, the implied dynamical mass contained within the central  $8''$  is  $\sim 0.6 - 1.6 \times 10^{12} M_{\odot}$ . The velocity dispersion of the Ly $\alpha$  emission line is large ( $\sigma \lesssim 400 \text{ km s}^{-1}$ ).

The source of the ionization for the nebula is ambiguous. The geometry of the emitting region and the shape of the SED suggest that the mid-infrared source SST24 J1434110+331733 is unlikely to be responsible for more than  $\sim 20\%$  of the Ly $\alpha$  luminosity, and it is likely that the ionization and line radiation are the result of shocks and / or multiple, distributed ionizing sources. If the Ly $\alpha$  emission is primarily powered by hot, young stars, the total star formation rate of the system is  $\sim 150 M_{\odot} \text{ yr}^{-1}$ . The detection of localized, weak, narrow C IV and He II emission near the center of the nebula suggests that at least portions of the nebula may be ionized by a power-law ionizing source or perhaps contain low metallicity gas; however, there is clearly  $24\mu\text{m}$  emission from other parts of the system that most likely is due to emission from dust, suggesting that the nebula is very inhomogeneous in its properties. It is likely that multiple sources of ionization exist within the nebula.

The mid-infrared source in the nebula is very luminous; if the SED is similar to Arp 220, the implied far-infrared luminosity is  $L_{\text{FIR}} \approx 5.8 \times 10^{13} L_{\odot}$ . The mid-infrared SED is well modelled as a power-law  $\propto \nu^{-2}$ , and bears more resemblance to the SEDs of active galaxies and quasars than to star-forming galaxies. We suggest that the MIPS source is a forming, enshrouded, AGN, perhaps similar to the  $z \sim 2.5$  extremely luminous dust-enshrouded AGN recently discovered through *Spitzer* IRS spectroscopy (Houck et al. 2005). Spectroscopy with *Spitzer* IRS will be necessary to determine the relative contributions of a hot dust continuum component and PAH emission to the total mid-IR flux, and will help us better constrain the relative roles of young stars and AGN in heating the dust.

Since the large Ly $\alpha$  nebula encompasses a revealed ‘Lyman Break galaxy’ and an enshrouded active region, we suggest a scenario in which the two objects represent sites of past and present galaxy formation and the Ly $\alpha$  emission traces the region of current infall. In a manner similar to that observed in nearby HII regions, the galaxy formation “front” in this system is moving gradually to the south (perhaps at a rate of  $\sim 300$  kpc Gyr $^{-1}$ ).

We speculate that Ly $\alpha$  nebulae such as this one may be found through their associated far-infrared emission. Although this may appear contradictory, it is quite plausible that both strong 24 $\mu$ m emission from dust (powered by enshrouded star-formation and/or accretion activity) and strong Ly $\alpha$  emission (powered by the cooling of gas in the deep potential well and perhaps by photoionizing radiation escaping from the enshrouded regions) are joint signposts for the spectacular events associated with the formation of the most massive galaxies.

This work is based in part on observations made with the Spitzer Space Telescope, which is operated by the Jet Propulsion Laboratory, California Institute of Technology under NASA contract 1407. We are grateful to the expert assistance of Paola Amico and Joel Aycocck at W. M. Keck Observatory and to the staff of Kitt Peak National Observatory where the Boötes field observations of the NDWFS were obtained. The authors thank NOAO for supporting the NOAO Deep Wide-Field Survey. In particular, we thank Lindsey Davis, Alyson Ford, Emma Hogan, Lissa Miller, Erin Ryan, Glenn Tiede and Frank Valdes for their able assistance with the NDWFS data. We also thank Ms. Miranda Nordhaus, Dr. Dianne Harmer, Dr. Richard Green and Dr. George Jacoby for enabling the WIYN observations discussed in this paper. AD thanks Joan Najita, Steve Strom and Joe Shields for useful discussions related to this system. We thank Rob Ivison, Henrik Spoon and Laura Silva for providing template SEDs. We thank an anonymous referee for useful comments. NOAO is operated by the Association of Universities for Research in Astronomy (AURA), Inc. under a cooperative agreement with the National Science Foundation. The authors also wish to recognize and acknowledge the very significant cultural role and reverence that the summit of Mauna Kea has always had within the indigenous Hawaiian community.

## REFERENCES

- Appleton, P. N., Fadda, D. T., Marleau, F. R., Frayer, D. T., Helou, G., Condon, J. J., Choi, P. I., Yan, L., Lacy, M., Wilson, G., Armus, L., Chapman, S. C., Fang, F., Heinrichson, I., Im, M., Jannuzi, B. T., Storrie-Lombardi, L. J., Shupe, D., Soifer, B. T., Squires, G., & Teplitz, H. I. 2004, *ApJS*, 154, 147
- Blain, A. W., Chapman, S. C., Smail, I., & Ivison, R. 2004, *ApJ*, 611, 725

- Chapman, S. C., Scott, D., Windhorst, R. A., Frayer, D. T., Borys, C., Lewis, G. F., & Ivison, R. J. 2004, *ApJ*, 606, 85
- de Vries, W. H., Morganti, R., Röttgering, H. J. A., Vermeulen, R., van Breugel, W., Rengelink, R., & Jarvis, M. J. 2002, *AJ*, 123, 1784
- Dey, A. 1999, in *The Most Distant Radio Galaxies*, 19–32
- Dey, A., Jannuzi, B. T., & et al. 2005, *ApJS*, in prep
- Dey, A., van Breugel, W., Vacca, W. D., & Antonucci, R. 1997, *ApJ*, 490, 698
- Dopita, M. A., & Sutherland, R. S. 1996, *ApJS*, 102, 161
- Eisenhardt, P. R., Stern, D., Brodwin, M., Fazio, G. G., Rieke, G. H., Rieke, M. J., Werner, M. W., Wright, E. L., Allen, L. E., Arendt, R. G., Ashby, M. L. N., Barmby, P., Forrest, W. J., Hora, J. L., Huang, J.-S., Huchra, J., Pahre, M. A., Pipher, J. L., Reach, W. T., Smith, H. A., Stauffer, J. R., Wang, Z., Willner, S. P., Brown, M. J. I., Dey, A., Jannuzi, B. T., & Tiede, G. P. 2004, *ApJS*, 154, 48
- Elmegreen, B. G., & Lada, C. J. 1977, *ApJ*, 214, 725
- Fazio, G. G., Hora, J. L., Allen, L. E., Ashby, M. L. N., Barmby, P., Deutsch, L. K., Huang, J.-S., Kleiner, S., Marengo, M., Megeath, S. T., Melnick, G. J., Pahre, M. A., Patten, B. M., Polizotti, J., Smith, H. A., Taylor, R. S., Wang, Z., Willner, S. P., Hoffmann, W. F., Pipher, J. L., Forrest, W. J., McMurty, C. W., McCreight, C. R., McKelvey, M. E., McMurray, R. E., Koch, D. G., Moseley, S. H., Arendt, R. G., Mentzell, J. E., Marx, C. T., Losch, P., Mayman, P., Eichhorn, W., Krebs, D., Jhabvala, M., Gezari, D. Y., Fixsen, D. J., Flores, J., Shakoorzadeh, K., Jungo, R., Hakun, C., Workman, L., Karpati, G., Kichak, R., Whitley, R., Mann, S., Tollestrup, E. V., Eisenhardt, P., Stern, D., Gorjian, V., Bhattacharya, B., Carey, S., Nelson, B. O., Glaccum, W. J., Lacy, M., Lowrance, P. J., Laine, S., Reach, W. T., Stauffer, J. A., Surace, J. A., Wilson, G., Wright, E. L., Hoffman, A., Domingo, G., & Cohen, M. 2004, *ApJS*, 154, 10
- Ferland, G. J. 1981, *ApJ*, 249, 17
- Francis, P. J., Williger, G. M., Collins, N. R., Palunas, P., Malumuth, E. M., Woodgate, B. E., Teplitz, H. I., Smette, A., Sutherland, R. S., Danks, A. C., Hill, R. S., Lindler, D., Kimble, R. A., Heap, S. R., & Hutchings, J. B. 2001, *ApJ*, 554, 1001

- Francis, P. J., Woodgate, B. E., Warren, S. J., Moller, P., Mazzolini, M., Bunker, A. J., Lowenthal, J. D., Williams, T. B., Minezaki, T., Kobayashi, Y., & Yoshii, Y. 1996, *ApJ*, 457, 490
- Haiman, Z. 2004, *ApJ*, 613, 36
- Haiman, Z., & Rees, M. J. 2001, *ApJ*, 556, 87
- Haiman, Z., Spaans, M., & Quataert, E. 2000, *ApJ*, 537, L5
- Heckman, T. M., Baum, S. A., van Breugel, W. J. M., & McCarthy, P. 1989, *ApJ*, 338, 48
- Houck, J. R., Soifer, B. T., Weedman, D., Higdon, S. J. U., Higdon, J. L., Brown, M. J. I., Dey, A., Jannuzi, B. T., Le Flo'c'h, E., Rieke, M., Armus, L., Charmandaris, V., Brandl, B. R., & Teplitz, H. I. 2005, *ApJ*, in press
- Iverson, R. J., Greve, T. R., Serjeant, S., Bertoldi, F., Egami, E., Mortier, A. M. J., Alonso-Herrero, A., Barmby, P., Bei, L., Dole, H., Engelbracht, C. W., Fazio, G. G., Frayer, D. T., Gordon, K. D., Hines, D. C., Huang, J.-S., Le Flo'c'h, E., Misselt, K. A., Miyazaki, S., Morrison, J. E., Papovich, C., Pérez-González, P. G., Rieke, M. J., Rieke, G. H., Rigby, J., Rigopoulou, D., Smail, I., Wilson, G., & Willner, S. P. 2004, *ApJS*, 154, 124
- Jannuzi, B. T., & Dey, A. 1999, in *ASP Conf. Ser. 191: Photometric Redshifts and the Detection of High Redshift Galaxies*, 111
- Jannuzi, B. T., Dey, A., & et al. 2005, *ApJS*, in prep
- Keel, W. C., Cohen, S. H., Windhorst, R. A., & Waddington, I. 1999, *AJ*, 118, 2547
- Kennicutt, R. C. 1983, *ApJ*, 272, 54
- Lacy, M., Storrie-Lombardi, L. J., Sajina, A., Appleton, P. N., Armus, L., Chapman, S. C., Choi, P. I., Fadda, D., Fang, F., Frayer, D. T., Heinrichsen, I., Helou, G., Im, M., Marleau, F. R., Masci, F., Shupe, D. L., Soifer, B. T., Surace, J., Teplitz, H. I., Wilson, G., & Yan, L. 2004, *ApJS*, 154, 166
- Landolt, A. U. 1992, *AJ*, 104, 340
- Madau, P., Pozzetti, L., & Dickinson, M. 1998, *ApJ*, 498, 106
- Massey, P., & Gronwall, C. 1990, *ApJ*, 358, 344
- Massey, P., Strobel, K., Barnes, J. V., & Anderson, E. 1988, *ApJ*, 328, 315

- Matsuda, Y., Yamada, T., Hayashino, T., Tamura, H., Yamauchi, R., Ajiki, M., Fujita, S. S., Murayama, T., Nagao, T., Ohta, K., Okamura, S., Ouchi, M., Shimasaku, K., Shioya, Y., & Taniguchi, Y. 2004, *AJ*, 128, 569
- McCarthy, P. J., Le Borgne, D., Crampton, D., Chen, H., Abraham, R. G., Glazebrook, K., Savaglio, S., Carlberg, R. G., Marzke, R. O., Roth, K., Jørgensen, I., Hook, I., Murowinski, R., & Juneau, S. 2004, *ApJ*, 614, L9
- McCarthy, P. J., Spinrad, H., Dickinson, M., van Breugel, W., Liebert, J., Djorgovski, S., & Eisenhardt, P. 1990, *ApJ*, 365, 487
- Monet, D. B. A., Canzian, B., Dahn, C., Guetter, H., Harris, H., Henden, A., Levine, S., Luginbuhl, C., Monet, A. K. B., Rhodes, A., Riepe, B., Sell, S., Stone, R., Vrba, F., & Walker, R. 1998, *VizieR Online Data Catalog*, 1252, 0
- Monet, D. G., Levine, S. E., Canzian, B., Ables, H. D., Bird, A. R., Dahn, C. C., Guetter, H. H., Harris, H. C., Henden, A. A., Leggett, S. K., Levison, H. F., Luginbuhl, C. B., Martini, J., Monet, A. K. B., Munn, J. A., Pier, J. R., Rhodes, A. R., Riepe, B., Sell, S., Stone, R. C., Vrba, F. J., Walker, R. L., Westerhout, G., Brucato, R. J., Reid, I. N., Schoening, W., Hartley, M., Read, M. A., & Tritton, S. B. 2003, *AJ*, 125, 984
- Nenkova, M., Ivezić, Ž., & Elitzur, M. 2002, *ApJ*, 570, L9
- Oke, J. B. 1990, *AJ*, 99, 1621
- Oke, J. B., Cohen, J. G., Carr, M., Cromer, J., Dingizian, A., Harris, F. H., Labrecque, S., Lucinio, R., Schaal, W., Epps, H., & Miller, J. 1995, *PASP*, 107, 375
- Padmanabhan, T. 2002, *Theoretical Astrophysics, Volume III: Galaxies and Cosmology* (*Theoretical Astrophysics, Volume III: Galaxies and Cosmology*, by T. Padmanabhan. *Theoretical Astrophysics*, 2002, 638 pp.)
- Palunas, P., Teplitz, H. I., Francis, P. J., Williger, G. M., & Woodgate, B. E. 2004, *ApJ*, 602, 545
- Papovich, C., Dickinson, M., & Ferguson, H. C. 2001, *ApJ*, 559, 620
- Pentericci, L., Kurk, J. D., Röttgering, H. J. A., Miley, G. K., van Breugel, W., Carilli, C. L., Ford, H., Heckman, T., McCarthy, P., & Moorwood, A. 2000, *A&A*, 361, L25
- Pentericci, L., Röttgering, H. J. A., Miley, G. K., Carilli, C. L., & McCarthy, P. 1997, *A&A*, 326, 580

- Pier, E. A., & Krolik, J. H. 1992, *ApJ*, 401, 99
- Reuland, M., van Breugel, W., Röttgering, H., de Vries, W., Stanford, S. A., Dey, A., Lacy, M., Bland-Hawthorn, J., Dopita, M., & Miley, G. 2003, *ApJ*, 592, 755
- Rieke, G. H., Young, E. T., Engelbracht, C. W., Kelly, D. M., Low, F. J., Haller, E. E., Beeman, J. W., Gordon, K. D., Stansberry, J. A., Misselt, K. A., Cadien, J., Morrison, J. E., Rivlis, G., Latter, W. B., Noriega-Crespo, A., Padgett, D. L., Stapelfeldt, K. R., Hines, D. C., Egami, E., Muzerolle, J., Alonso-Herrero, A., Blaylock, M., Dole, H., Hinz, J. L., Le Floch, E., Papovich, C., Pérez-González, P. G., Smith, P. S., Su, K. Y. L., Bennett, L., Frayer, D. T., Henderson, D., Lu, N., Masci, F., Pesenson, M., Rebull, L., Rho, J., Keene, J., Stolovy, S., Wachter, S., Wheaton, W., Werner, M. W., & Richards, P. L. 2004, *ApJS*, 154, 25
- Schaerer, D. 2002, *A&A*, 382, 28
- . 2003, *A&A*, 397, 527
- Shapiro, S. L. 2005, *ApJ*, 620, 59
- Shapley, A. E., Steidel, C. C., Pettini, M., & Adelberger, K. L. 2003, *ApJ*, 588, 65
- Silva, L., Granato, G. L., Bressan, A., & Danese, L. 1998, *ApJ*, 509, 103
- Spoon, H. W. W., Moorwood, A. F. M., Lutz, D., Tielens, A. G. G. M., Siebenmorgen, R., & Keane, J. V. 2004, *A&A*, 414, 873
- Steidel, C. C., Adelberger, K. L., Shapley, A. E., Pettini, M., Dickinson, M., & Giavalisco, M. 2000, *ApJ*, 532, 170
- . 2003, *ApJ*, 592, 728
- Stern, D., Eisenhardt, P., Gorjian, V., Kochanek, C. S., Eisenstein, D., Brodwin, M., I., B. M. J., Caldwell, N., Cool, R., Dey, A., Green, P., Jannuzi, B. T., Murray, S. S., Pahre, M. A., & Willner, S. P. 2005, *ApJ*, XXX
- Stone, R. P. S. 1977, *ApJ*, 218, 767
- Storey, P. J., & Hummer, D. G. 1995, *MNRAS*, 272, 41
- Sutherland, R. S., & Dopita, M. A. 1993, *ApJS*, 88, 253
- Taniguchi, Y., & Shioya, Y. 2000, *ApJ*, 532, L13

- van Ojik, R., Röttgering, H. J. A., Miley, G. K., & Hunstead, R. W. 1997, *A&A*, 317, 358
- Villar-Martín, M., Vernet, J., di Serego Alighieri, S., Fosbury, R., Humphrey, A., & Pentericci, L. 2003, *MNRAS*, 346, 273
- Villar-Martín, M., Vernet, J., di Serego Alighieri, S., Fosbury, R., Pentericci, L., Cohen, M., Goodrich, R., & Humphrey, A. 2002, *MNRAS*, 336, 436
- Yoo, J., & Miralda-Escudé, J. 2004, *ApJ*, 614, L25
- Zirm, A. W., Dickinson, M., & Dey, A. 2003, *ApJ*, 585, 90

Table 2. Emission-Line Strengths<sup>a</sup>

Line	Obs. Wavelength (Å)	Aperture ( $''$ )	Flux ( $\text{erg s}^{-1} \text{cm}^{-2}$ )	FWHM (Å)	Obs. EW (Å)	Luminosity <sup>b</sup> ( $\text{erg s}^{-1}$ )
Ly $\alpha$	4448	10.0 radius <sup>c</sup>	$2.89 \pm 0.15 \times 10^{-15}$	-	-	$1.67 \times 10^{44}$
Ly $\alpha$	4444.7	10.9 $\times$ 1.5	$4.05 \pm 0.01 \times 10^{-16}$	13.0	316	$2.33 \times 10^{43}$
Ly $\alpha$	4445.0	4.5 $\times$ 1.5	$3.10 \pm 0.01 \times 10^{-16}$	12.8	396	$1.79 \times 10^{43}$
NV	-	4.5 $\times$ 1.5	$< 5.1 \times 10^{-18}$ <sup>d</sup>	-	$< 7.3$	
C IV	5662.0	4.5 $\times$ 1.5	$4.17 \pm 0.04 \times 10^{-17}$	15.2 <sup>e</sup>	85	$2.40 \times 10^{42}$
He II	5997.9	4.5 $\times$ 1.5	$4.07 \pm 0.04 \times 10^{-17}$	7.3	60	$2.35 \times 10^{42}$
C III]	6974.6	4.5 $\times$ 1.5	$5 \pm 1 \times 10^{-18}$	$< 13$		$4.6 \times 10^{41}$
-	5081.6	4.5 $\times$ 1.5	$5.15 \pm 0.04 \times 10^{-17}$	$< 4$	87	

<sup>a</sup>All quantities are measured from the PA=19.4° spectrum with the exception of the first entry in the table, which is measured from the narrow-band image.

<sup>b</sup> Luminosities are calculated for a cosmology with  $H_0 = 70 \text{ km s}^{-1} \text{ Mpc}^{-1}$ ,  $\Omega_m = 0.3$ ,  $\Omega_\lambda = 0.7$ .

<sup>c</sup>Measured from the narrow-band image after subtracting the continuum flux estimated from the G-band image

<sup>d</sup>Upper limits quoted are  $3\sigma$  and assume lines of the same width as the He II feature.

<sup>e</sup>C IV width is measured by modelling the doublet as a single feature.